Amyotrophic Lateral Sclerosis associated variants of *CFAP410* affect the DNA damage response leading to Motor neuron degeneration

Ross Ferguson
University of Bath
Vasanta Subramanian (bssvss@bath.ac.uk)
University of Bath https://orcid.org/0000-0002-1969-7333

Article

Keywords:

Posted Date: May 11th, 2022

DOI: https://doi.org/10.21203/rs.3.rs-1642268/v1

Abstract

Mutations in CFAP410, a basal body protein known to be required for the formation of primary cilia, have been recently identified in amyotrophic lateral sclerosis (ALS), a devastating late onset neurodegenerative disorder with poor prognosis. CFAP410 is also implicated in the DNA damage response and interacts with Nek1 also shown to be mutated in ALS. In this study we have investigated the effect of knocking in a HA epitope tag and two ALS associated mutations into the endogenous *Cfap410* gene by gene editing using CRISPR/Cas9 in mouse embryonic stem cells (mESCs). We show that primary cilia in these mESCs, the neural progenitors and neurons differentiated from these mESCs do not exhibit any gross abnormalities. However, ESCs, neural progenitors and neurons with knockin *Cfap410* ALS variants are more susceptible to DNA damage and exhibit impaired interaction with Nek1. Our findings point to DNA damage as a convergent pathway leading to ALS.

Introduction

Amyotrophic lateral sclerosis (ALS) is a fatal neurodegenerative disorder affecting upper and lower motor neurons with a prevalence of between 3 to 5 per 100000 persons worldwide and this incidence is on the increase (Chio et al, 2013; Brown and Chalabi, 2017; Hardimann et al., 2017). Several new causative/risk genes have been/are being identified for ALS (Chia et al 2018, van Rheenen et al 2021, Zhang et al, 2022) and one of these is the Cilia and Flagella associated protein 410 (*CFAP410*- alias *C21orf2;* van Rheenan et al., 2016). Besides ALS, mutations in *CFAP410* have also been reported in ciliopathies such as Axial spondylometaphyseal dysplasia, Jeune syndrome and retinal dystrophy (Thiel et al., 2011; Wheway et al.,2015, Wang et al., 2016, Khan et al., 2015, Schmidts et al., 2013).

The biological function of CFAP410 is not particularly well understood. It appears to be essential for primary cilia formation (Shalom et al., 2008) and has also been shown to play a role in the organization of the actin cytoskeleton (Bai et al., 2011). Immuno-histochemical studies in human, pig and mouse retinas localised the CFAP410 protein to the ciliary structures of the photoreceptor cells (Schmidts et al., 2013). Expression of *CFAP410* is also seen in the brain and spinal cord (FANTOM5 and MGI Gene Expression Database) and shown to localize to mitochondria in immune cells. The expression of *CFAP410* in the brain and spinal cord and the occurrence of variants seen in ALS suggests that *CFAP410* has an important role to play in the nervous system. CFAP410 is also likely to be a part of the ciliary structures of cells in the brain.

Primary cilia play a key role in transducing signals particularly of the sonic hedgehog signaling pathway. This pathway plays a key role in the normal development of the central nervous system particularly the hippocampus, cerebellum and spinal cord (Fliegauf, et al, 2007). Loss of *CFAP410* in siRNA-treated IMCD3 cells led to either complete loss of cilia and/or a few cilia reduced to stumps (≤1.5 μm). Thus, it appears that CFAP410 is required for elongation of primary cilia as well as for Shh signalling (Lai, et al, 2011).

CFAP410 interacts and forms a functional complex with never in mitosis gene A related kinase 1 (NEK1; Wheway et al., 2015). NEK1 ALS risk variants have been reported in both familial and sporadic cases of ALS (Brenner et al., 2016; Gratten et al., 2017; Kenna et al., 2016). NEK1 possess both serine threonine and tyrosine kinase activities and plays an important role in the regulation of the cell cycle and DNA damage repair (Chen et al., 2008; Fry et al., 2012; Melo-Hanchuk et al., 2017). An ALS variant in this gene leads to increased DNA damage in patient derived motor neurons (Higelin et al, 2018). Like NEK1, CFAP410 has also been implicated in DNA repair mechanisms (Fang et al., 2015) and more recently the V58L ALS variant of CFAP410 has been shown to be stabilised upon hyperphosphorylation by NEK1 (Watanabe et al, 2020). Taken together, it is likely that the ALS variants seen in the conserved domains of CFAP410 such as the LRR- domains (protein interaction domains) may affect primary cilia and/or the actin cytoskeleton thereby affecting neurons. Furthermore, because of its role in DNA repair mechanism, CFAP410 ALS variants neurons may exhibit an aberrant DNA damage response.

The variants in CFAP410 associated with ALS occur throughout the protein and many of these are rare variants (van Rheenan et al., 2016). At present it is unclear which of these are risk variants relevant to the aetiology of ALS. A comparison of the amino acid sequence of CFAP410 reveals that there is significant conservation across species. There are two major regions of conservation (1) an N-terminal conserved region (1–142 aa, coded by exons 1–5) where there is a predicted mitochondria localization signal peptide, two tandem leucine-rich repeat 4 (LRR4, residues 40-80) domains followed by a leucine-rich repeat cap (LRR cap, residues 104-122) and (2) a short conserved stretch at the C-terminus (214–256 aa ,encoded by exon 7). Neither the C-terminal conserved region nor the variable region, exhibit any homology to known domains and proteins.

Using a bioinformatics and structure homology modelling approach we have previously predicted changes in local interactions for the different ALS risk variants of conserved residues of CFAP410 (Iyer et al 2018). Here in this report, we have chosen to study the effects of two of these ALS associated variants- V20M and R73P on neuroepithelial cells and motor neurons. In order to do this, we have used a gene editing approach to introduce the *CFAP410* ALS variants into the endogenous mouse *Cfap410* gene instead of overexpressing these, so as to have a physiologically relevant model which recapitulates the effects seen in human ALS.

Herein, we have modified the coding sequence of the endogenous *Cfap410* gene in mouse ES cells to include the hemagglutinin (HA) epitope tag at the 3’ end of the protein. Subsequently, we have introduced mutations into the coding sequence at positions homologous to two of the mutations which have been associated with amyotrophic lateral sclerosis in human patients (van Rheenan et al., 2016). We have found that the ES cell derived motor neurons carrying either of the two ALS associated mutation are susceptible to DNA damage and have an impaired DNA damage response.

Results

Cfap410 transcript 1 is the major protein coding transcript in the developing brain and differentiating motor neurons

Ensembl shows eight mouse *Cfap410* transcripts (1810043G02Rik) with two protein coding variants: 1810043G02Rik-201 encoding the 249aa isoform (Uniprot Q8C6G1) and 1810043G02Rik-202 encoding the 212aa isoform (Uniprot Q3U699).

To ensure the most relevant transcript was tagged with the HA epitope, we first studied the expression of the different *Cfap410* transcripts in a developmental series of mouse brain tissue and in motor neurons differentiated in vitro from P19 embryonal carcinoma cells. Expression of transcript 1 (Rik-201) increases only slightly during early embryonic brain development between E12.5 and E16.5. A more dramatic increase is seen from E16.5 to E18.5 which then continues postnatally to P0 and P15 in the cerebrum with a threefold increase over E12.5 expression levels (Figure S1a). This is not observed in the cerebellum though there is still a gradual increase in expression up to P15. A similar trend is seen after E18.5 for transcript two (Rik-202) in the cerebrum, though at lower absolute levels (Figure S1b).

Cfap410 transcript 1 expression also shows a similar expression pattern in differentiating P19 cells (Figure S1c). First there is a gradual increase in expression up to the midpoint of the differentiation then a more rapid increase to levels two-fold higher than those seen in undifferentiated P19 cells. Little change is observed in the case of transcript two in differentiating P19 cells (Figure S1d). These data suggest transcript 1 and therefore the 249aa isoform of Cfap410 is the dominant isoform in the developing brain and differentiating motor neurons. Therefore, we chose to introduce the HA epitope tag into this isoform.

Design of guides and screening of sgRNA pairs for efficiency in mESC

Four pairs of guides were designed to target nickase Cas9 (nCas9) to the positions at which edits were to be introduced into the *Cfap410* gene: A C-terminal HA epitope tag (Figure 1a) and point mutations resulting in residue changes V20M and R73P homologous to those identified in patients (Figure 1b & c). These guide pairs were screened for their efficiency by assaying the frequency of indels in pools of transiently transfected R1 mESCs. Transfection efficiency was monitored by co-transfection with a fluorescent reporter construct (pCagTag, Trichas et al., 2008). Gene editing frequency was determined after 24h using the T7E1 endonuclease assay on PCR products spanning the intended edit sites. (Vouillot et al., 2015). The following guide pairs were identified as the most efficient of each set associated with an intended insertion or mutation: ‘HA tag’ sgRNAs 18-11, ‘V20M’ sgRNAs 5-2 and ‘R73P’ sgRNAs 6-7 (Figure S2a-c) and shown as highlighted in Table S2 in Supplementary materials.

Knockin of a HA epitope tag and ALS associated mutations into the *Cfap410* gene in mESCs.

The *Cfap410* gene was edited in R1 mESCs to introduce the HA epitope tag in either one or both alleles (Figure 1a). This was followed by the introduction of point mutation resulting in residue changes homologous to those identified in patients: V20M and R73P (Figure 1b & c).

We first introduced the HA tag prior to the stop codon in the final coding exon of transcript 1 of *Cfap410* in R1 mESCs as described in Materials and Methods. Transfected ES cell clones were picked and expanded (Figure 1a). Clones were screened by PCR for successful introduction of the HA tag using a primer specific to the HA tag and a second to the endogenous *Cfap410* gene. Out of 576 clones screened, six were positive for the HA tag. These clones were expanded and characterised further by PCR to amplify products that span from the HA tag to endogenous sequence (i.e. outside of the homology arms present in the donor plasmid) indicate the tag is present in the intended genomic site and not randomly inserted elsewhere.

In addition to the HA tag, the donor plasmid introduces a novel EcoRI site outside of the coding sequence (Figure 1d). This was used to determine the zygosity of the knock-in. Using the primer pair described for the T7E1 assay, a fragment spanning the stop codon was amplified. This PCR product was subsequently digested with EcoRI; homozygotes will show completely digested products while heterozygotes will show only half. Two clones appeared to be homozygous for the HA tag while the remaining four appear to be heterozygous (Figure 1d). Some smearing of the PCR product was observed prior to digestion in some clones, which suggested the presence of indels in the WT allele in some clones.

The PAM site in the knock-in allele was mutated to prevent further editing. In order to verify that the wild type allele in heterozygous clones had no mutations/deletions, the HA spanning PCR products generated from DNA of these clones were subcloned into pBluescript. After transformation, eight clones from each transformation were subjected to colony PCR to amplify the cloned fragment and the product digested with EcoRI. Clones which showed no change after digest were sequenced. One heterozygous clone showed no indels in the second allele, two carried WT coding sequences but deletions in the 3'UTR and the last carried a deletion spanning the stop codon (Figure S2e). Heterozygous *CFAP410*-HA clones with deletions in the wild type allele were excluded from subsequent experiments. Expression of the HA tagged Cfap410 isoform was confirmed by Western blot where a band at 29kDa is observed (Figure 1e).

Disease associated mutations were then introduced into R1 *Cfap410* HA tagged clones which were either homo- or heterozygous for the HA tag (i.e. $CFAP410^{HA/HA}$ or $CFAP410^{+/HA}$) in order to generate cell lines carrying heterozygous or homozygous HA tagged variants. The donor constructs for generating the V20M and R73P mutations were introduced by electroporation into R1 $Cfap410^{HA}$ tagged mESC clones. Clones were picked as before after puromycin selection and magnetic sorting. To screen for the presence of the knock-in, clones were first screened by melt curve analysis. This was done by PCR spanning the targeted site. The introduction of the point mutation, synonymous MseI site and PAM mutation result in

characteristic changes in the melt profile of PCR fragments after amplification, which was confirmed by digestion with MseI.

Seven hundred and sixty-eight clones isolated were screened from the R1 *Cfap410*$^{+/HA}$ transfection with the V20M donor construct, guides and nCas9. One hundred and twenty of these clones (15.6%) had altered melt curves after MseI digest suggesting successful editing had occurred. Of the 768 clones screened from the R1 *Cfap410*$^{HA/HA}$ transfection, 8.8% showed altered melt curves. Similar frequencies were observed during construction of the R73P lines.

These clones were expanded further and characterised for the nature of the edit or mutations that were present. Gel analysis of the clones identified by melt-curve analysis identified homozygous V20M or R73P mutations in transfected subclones of *Cfap410*$^{HA/HA}$ R1 mESCs where complete digestion of the PCR amplicon by MseI occurred (i.e., *Cfap410*$^{V20M\text{-}HA/V20M\text{-}HA}$ or *Cfap410*$^{R73P\text{-}HA/R73P\text{-}HA}$). Similarly, a correctly sized wild-type allele band and an MseI digested bands were used to further screen for heterozygous V20M or R73P mutations in transfected subclones of *Cfap410*$^{+/HA}$ R1 mESCs. The presence of the mutations were verified by Sanger sequencing, showing both the intended mutation and an intact wild-type allele in heterozygous clones (Figure S2f and g). Heterozygous point mutations could have occurred in either the wild-type or HA tagged allele of *Cfap410*$^{+/HA}$ cells. In order to determine which allele carried the mutation, cDNA from prospective clones was subjected to PCR using *Cfap410* transcript 1 forward primer combined with a HA tag reverse primer followed by digestion with MseI. PCR products from heterozygous clones produced digested products only when the novel MseI site was present in the amplicon i.e. the point mutation was present in the HA tagged allele (i.e. *Cfap410*$^{+/V20M\text{-}HA}$ or *Cfap410*$^{+/R73P\text{-}HA}$ (Figure 1h). Table 1 shows the two independent clones of each genotype that were taken forward for further analysis.

Cfap410-HA variant proteins are stable and associate with pericentrin

Knocking in the point mutations R73P and V20M into the *Cfap410* gene in undifferentiated mESCs did notappear to affect the stability or levels of the HA tagged Cfap410 protein under normal culture conditions (Figure 2a-b). Levels of Cfap410 variant proteins in homozygous *Cfap410*$^{V20M/V20M\text{-}HA/HA}$ or *Cfap410*$^{R73P/R73P\text{-}HA/HA}$ cell lines was comparable to that seen in the parent cell line R1*Cfap410*$^{HA/HA}$. Clones heterozygous for either V20M or R73P mutation showed protein levels approximately half the levels of Cfap410 seen in the homozygous clones (Figure 2 and b).

Immunostaining for the HA tag revealed staining in small punctae found primarily throughout the cytoplasm but also within the nucleus (Figure 2c). Co-staining with the centrosomal marker pericentrin

(PCNT) identified an association of larger punctae with the centrosome (Figure 2c, insets). No gross differences in distribution of the HA tag staining or association with PCNT were observed between wildtype *Cfap410*$^{+/HA}$ and *Cfap410*$^{HA/HA}$ ESCs and the ESCs carrying the Knockin HA tagged ALS variants.

Known protein-protein interactions are disrupted by ALS associated Cfap*410* mutations

The anti HA tag antibody was used to immunoprecipitate WT-HA, V20M-HA and R73P-HA Cfap410 proteins from neuronal cells differentiated from the parental R1 *Cfap410*$^{WT/WT}$, *Cfap410*$^{HA/HA}$, *CFAP410*$^{V20M\text{-}HA/V20M\text{-}HA}$ and *CFAP410*$^{R73P\text{-}HA/R73P\text{-}HA}$ ESCs. The co-immunoprecipitation of proteins reported to interact with *CFAP410* (NEK1, SPATA7 and FBXO3, (Fang et al., 2015; Wheway et al., 2015a; Watanabe et al., 2020;) (Figure 2d). Co-immunoprecipitation confirmed these interactions occurred in the *Cfap410* ALS variant knockin cells regardless of genotype (Figure 2e-h). However, quantitation by densitometry indicated reduced interactions between *Cfap410*$^{R73P\text{-}HA}$ and NEK1, SPATA7 and FBXO3 in two independent clones tested (Figure 2e-h, $P<0.05$).

CFAP410 variants do not affect the frequency of primary cilia.

Previous reports have suggested CFAP410 is involved in the formation or maintenance of the primary cilia (Khan et al., 2015; Wheway et al., 2015b). To examine whether primary cilia were affected in cells with the knockin *Cfap410* ALS variants, ciliogenesis was induced in ESCs and NPCs either through serum starvation or the removal of EGF & FGF2, respectively (Figure S3a & b). Primary cilia frequency within the total population of cells was determined by staining with anti ARL13B antibody. ARL13B is a small GTPase that localizes to the ciliary axoneme (Li et al., 2012). No significant differences were found in the frequency of cells with primary cilia between the control and *Cfap410* ALS variant knockin ESCs or NPCs (Figure S3d & e).

In neuronal cultures, few ISL1/2 positive motor neurons possessed primary cilia in comparison to the total population (Figure S3c). Again, no significant difference in the frequency of primary cilia was observed between neurons/motor neurons derived from *Cfap10*$^{WT/WT}$ and *Cfap410*$^{HA/HA}$ clones and those carrying hetero- or homozygous $^{V20M\text{-}HA}$ or $^{R73P\text{-}HA}$ alleles (Figure S3f). Furthermore, no clear differences in length or morphology of primary cilia was observed by staining the axoneme with antibody

to ARL13B.. We also did not observe co-localisation between the mitochondrial marker MitoTracker and wild-type HA tagged *Cfap410* or any of the variants in neurons and their neurites (Figure S4).

Cfap410 variants do not affect ESC or NPC growth rates.

Proteins associated with primary cilia often play a role in cell division and proliferation. Although primary cilia frequency and morphology appear unaltered, defects may still be present in cilia-associated processes. We first examined whether ALS-associated mutations in *Cfap410* would affect the rate of proliferation in ES cells as well as neural progenitor cells (NPCs) derived from these ES cells.

Proliferation was assayed by measuring the viable cell population using an MTT based assay at 24h intervals after seeding each cell line at equal densities. At each interval during the four day period during which ES cell proliferation was assayed, both R1 *Cfap410*$^{WT/WT}$ and R1 *Cfap410*$^{HA/HA}$ cell lines showed comparable cell density, with some plateauing in growth rate after 72h (Figure 3a). In contrast, the heterozygous *Cfap410*$^{WT/V20M\text{-}HA}$ and *Cfap410*$^{WT/R73P\text{-}HA}$ cell lines showed a trend of reduced cell density at comparable time points (Figure 3a). This trend continued with the homozygous *Cfap410*$^{V20M\text{-}HA/V20M\text{-}HA}$ and *Cfap410*$^{R73P\text{-}HA/R73P\text{-}HA}$. However, no significant difference between the rates of proliferation was observed between any cell line (0.553-0.677 ΔA/24h by MTT between days 1 & 3) and differences in cell density were only observable after 24h (Figure 3a).

ES cells of each genotype were differentiated to NPC identity, expanded and characterised to ensure comparisons were being made between equivalent cell populations. Regardless of genotype, qRT-PCR showed no significant difference in expression of the NPC markers *Nestin*, *Pax6* and *Sox2* (Figure S5a). In addition, each clone expressed the intermediate filament nestin in characteristic NPC-like distribution (Figure S5b).

The growth characteristics of the NPCs followed a pattern similar to those observed for ES cells (Figure 3b). Over the six day time course, the density of *Cfap410*$^{WT/WT}$ and *Cfap410*$^{HA/HA}$ NPCs were consistently above those of *CFAP410*$^{WT/V20M\text{-}HA}$ and *CFAP410*$^{WT/R73P\text{-}HA}$ NPCs. Homozygous *CFAP410*$^{V20M\text{-}HA/V20M\text{-}HA}$ and *CFAP410*$^{R73P\text{-}HA/R73P\text{-}HA}$ NPCs had the lowest densities at each time point. Despite this proliferation rates were not significantly different (0.171-0.221 ΔA/24h by MTT between days 2 and 5, Figure 3b) and the differences in cell density appear to stem from the earliest time point.

Colony formation assays were performed for both ESC and NPC, to further investigate growth characteristics. The frequency of colonies formed negatively correlated with zygosity (Figure 3c & d). The downward trend in colony frequency observed for the two *CFAP410*$^{WT/V20M\text{-}HA}$ ESC lines was not significantly different from that of the *CFAP410*$^{WT/WT}$ and *CFAP410*$^{HA/HA}$ ESCs (Figure 3e). The reduction in colony frequency for the *CFAP410*$^{WT/R73P\text{-}HA}$ ESC lines assayed was only significant in the case of one

of the two lines (M08, P<0.05). In contrast, the colony frequencies were halved where the ES cells were homozygous for both the *CFAP410*$^{V20M\text{-}HA}$ and *CFAP410* $^{R73P\text{-}HA}$ encoding alleles (P<0.05, Figure 3e). Similar results were observed for colony frequency in assays performed with the equivalent genotypes of NPCs (Figure 3f). Despite these differences in colony frequency, no significant differences were found between the median diameters of the colonies that did arise during the assays for with ESCs or NPCs of any genotype (median ESC colony diameter 122.2μm, σ 18.1 μm; Median NPC colony diameter 95.9 μm, σ 7.1 μm) (Figure 3g and h). This corresponds with the data showing no difference in proliferation rates between the different genotypes in both ESC and NPCs. These data suggest that the lag in growth observed during the early stages of the proliferation assays is likely due to increased cell death post-plating reducing the initial population size, potentially due to increased sensitivity to stress during passaging and plating at low starting densities.

ESCc, NPCs and neurons carrying *Cfap410* ALS variant knock-ins are more sensitive to stress in a zygosity-dependent manner.

Sensitivity to stress was assayed in neuronal populations differentiated to dorsal spinal identities, containing ~40% motor neurons (Figure 4). We also examined whether sensitivity to stress manifested in ESCs and NPCs (Figure S6).

In order to assay differences in the sensitivity of cells to stress, we generated dose response curves for three different stressors: the ROS-generating oxidative stressor sodium arsenite (ARS) (Hu et al., 2020), the topoisomerase II inhibitor Etoposide (ETO) which promotes DNA double strand breaks (Tammaro et al., 2013); and mitochondrial stressor valinomycin, which uncouples K^+ transport across membranes (Huang et al., 2021). ESCs, NPCs and neurons were subjected to varying concentrations of each stressor and cell viability was determined 24 hours later by MTT assay (Figure S5 and S6).

Cultures of motor neurons differentiated from *Cfap410* variant ESCs were consistently more vulnerable to each stressor (a lower [EC50]) than the equivalent from wild-type ESCs (Figure 4). In the case of each drug, a lower [EC50] was observed where the variant was present homozygously in comparison to heterozygotes. While the mean [EC50] for the wild-type HA tagged clones was 3.85, 2.44 & 0.81μM of ETO, VAL & ARS respectively, lower mean [EC50] were observed for the heterozygous *Cfap410*$^{+/V20M\text{-}HA}$ clones (ETO: 2.15 μM, VAL: 2.13 μM, ARS: 0.58 μM) and *Cfap410*$^{+/R73P\text{-}HA}$ clones (ETO: 1.83 μM, VAL: 2.00 μM, ARS: 0.68 μM). [EC50] were lower still in the case of *Cfap410*$^{V20M\text{-}HA/V20M\text{-}HA}$ clones (ETO: 1.24 μM, VAL: 1.29 μM, ARS: 0.51 μM) and *Cfap410*$^{R73P\text{-}HA/R73P\text{-}HA}$ clones (ETO: 1.28 μM, VAL: 1.35 μM, ARS: 0.53 μM). We did not observe any difference between the two different variants (V20M or R73P) to the effects of the drug in these assays. The same trends were observed in both *Cfap410* variant ESCs and NPCs ([EC50] values are summarised in Figure 4b, full kill curves can be found in Figure S6).

Motor neurons carrying *Cfap410* ALS variants are more vulnerable to stress

The differentiation protocol we used directs ESCs towards motor neuron identity however the resulting neuronal populations are not pure (Figure 5a). Within the differentiated cultures, motor neurons were identified by their expression of the transcription factors islet-1/2 (ISL), and the intermediate filament peripherin (PRPH) (Thiyagarajan et al., 2012). We did not find any significant differences in the frequency of ISL^+ neurons between *Cfap410*$^{WT/WT}$ or *Cfap410*$^{HA/HA}$ cultures and the hetero- or homozygous *Cfap410* ALS variant carrying neurons under normal culture condition (Figure 5b).

To investigate the effects of stress on motor neuron survival, cultures were treated with ETO, VAL or ARS at concentrations equivalent to the respective mean IC50 values determined for *Cfap410* variant cultures. In all cases, motor neurons were more vulnerable than the total neuronal population as fewer motor neurons survive after drug treatment. Motor neurons homozygous for *Cfap410* ALS variants were more susceptible to drug treatment. ETO, VAL and ARS treatment reduced the mean motor neuron frequencies of the control *Cfap410*$^{WT/WT}$ or *Cfap410*$^{HA/HA}$ cultures to 29% (σ 4.8%), 27% (σ 7.5%) & 30% (σ 4.2%) respectively (Figure 5b). ETO treatment significantly reduced the frequency of motor neurons to below 15% in *Cfap410*$^{V20M\text{-}HA/V20M\text{-}HA}$ (Clone C15 $\bar{x}$ 13.6%, σ 9.3%; Clone F02 $\bar{x}$ 14.8%, σ 3.4%) and *Cfap410*$^{R73P\text{-}HA/R73P\text{-}HA}$ (Clone D14 $\bar{x}$ 9.1%, σ 3.7%; Clone J13 $\bar{x}$ 13.9%, σ 6.7%) (Figure 5c, P<0.005). Similar trends were seen with VAL and ARS treatments. With VAL treatment, mean frequency of surviving motor neurons in the case of *Cfap410*$^{V20M\text{-}HA/V20M\text{-}HA}$ cultures was 8.6% (C15, σ 4.0%) and 11.7% (F02, σ 2.2%). In the case of *Cfap410*$^{R73P\text{-}HA/R73P\text{-}HA}$ cultures the mean frequency of surviving motor neurons was 11.2% (D14, σ 4.7%) and 10.9% (J13, σ 8.2%) (Figure 5d, P<0.005). With ARS treatment, the mean survining motor neuron frequencies in *Cfap410*$^{V20M\text{-}HA/V20M\text{-}HA}$ cultures was 10.9% (C15, σ 2.7%) and 13.8% (F02, σ 9.6%) and in the case of *Cfap410*$^{R73P\text{-}HA/R73P\text{-}HA}$ cultures was 7.9% (D14, σ 4.7%) and 7.6% (J13, σ 4.0%) (Figure 5e, P<0.005).

Surviving motor neuron frequency was also reduced in heterozygote cultures compared to wildtype, but not to the same extent as in homozygote cultures. ETO treatment reduced the mean motor neuron frequency in *Cfap410*$^{WT/V20M\text{-}HA}$ cultures to 22.0% (C13, σ 4.8%) and 21.2% (E09, σ 4.9%), and in *Cfap410*$^{WT/R73P\text{-}HA}$ cultures to 19.9% (B24, σ 7.4%) and 22.5% (M04, σ 12.2%) (Figure 5c, P<0.05). VAL treatment reduced the mean motor neuron frequency in *Cfap410*$^{WT/V20M\text{-}HA}$ cultures to 20.4% (C13, σ 1.8%) and 17.5% (E09, σ 4.2%), and in *Cfap410*$^{WT/R73P\text{-}HA}$ cultures to 18.1% (B24, σ 5.9%) and 22.6% (M04, σ 4.6%) (Figure 5d, P<0.05). Finally, ARS treatment reduced the mean motor neuron frequency in *Cfap410*$^{WT/V20M\text{-}HA}$ cultures to 25.9% (C13, σ 5.8%) and 25.1% (E09, σ 2.3%), and in *Cfap410*$^{WT/R73P\text{-}HA}$ cultures to 20.8% (B24, σ 1.3%) and 24.3% (M04, σ 6.9%) (Figure 5d, P<0.05).

No significant differences were found between motor neuron frequency in *Cfap410*$^{HA/V20M-HA}$ and *Cfap410*$^{HA/R73P-HA}$ cultures treated with ETO or VAL. A higher frequency of motor neurons in *Cfap410*$^{HA/V20M-HA}$ cultures survived relative to *Cfap410*$^{WT/WT}$ or *Cfap410*$^{HA/HA}$ cultures after ARS treatment in comparison to ETO or VAL. A similar trend is also observed in ARS treated homozygous *Cfap410*$^{V20M-HA/V20M-HA}$ in comparison to the *Cfap410*$^{R73P-HA/R73P-HA}$. This suggests that the V20M mutation has a less severe effect on Cfap410 function in response to certain types of stress.

During apoptosis, caspase-3 (CASP3) is cleaved and translocates to the nucleus (Jänicke et al., 1998). Immunostaining for cleaved caspase-3 (cCASP3) in neuronal cultures treated with drugs shows robust nuclear localisation, with many cells also showing condensed fragmented DNA seen by DAPI staining (Figure 6 and S7).

Co-immunostaining for cCASP3 and ISL1/2 failed to show cells both expressing the motor neuron marker with nuclear cCASP3. This may be because vulnerable motor neurons have apoptosed and been lost prior to fixation and observation at this time point, or ISL1/2 may have already been degraded during apoptosis in the remaining cells positive for nuclear cCASP3. Despite this, the frequency of cCASP3 present in the total neuronal population after drug treatment correlates with degree of motor neuron loss observed in Figure 5. Untreated neuronal cultures shown around 1-7% cCASP3 positive nuclei, with homozygous *Cfap410* variant neurons trending higher but not significantly so. After treatment with ETO, 5-15% of nuclei in *Cfap410*$^{WT/WT}$ and $^{HA/HA}$ cultures are cCASP3^{+} while 3-4 fold more neuronal nuclei are cCASP3^{+} in both homo- and heterozygous *Cfap410* variant neuronal cultures ($P<0.05$, Figure 5c), particularly in the case of both *Cfap410*$^{R73P-HA/R73P-HA}$ clones ($P<0.005$). Similar trends were seen after treatment with VAL and ARS, however, fewer cCASP3^{+} nuclei were observed in heterozygous *Cfap410* variant neurons when compared to *Cfap410* homozygous neurons as compared with ETO treatment. Neurons homozygous for the *Cfap410*$^{V20M-HA}$ and *Cfap410R*$^{73P-HA}$ ALS variants had an increased frequency of cCASP3^{+} nuclei.

Redistribution of nuclear TDP-43 to the cytoplasm is observed in nearly 97% of ALS patients (Suk and Rousseaux, 2020). In order to see if this happened in neurons with the knockin Cfap410 ALS variants, we stained for TDP-43 in control and *Cfap410* ALS variant neurons. TDP-43 was observed at low frequency in the soma of control neurons after treatment with ETO (Figure 6b,f-h), VAL and ARS (~2-4%, Figure S7b). The frequency of neurons in which this was observed was higher in the heterozygous *Cfap410*$^{HA/V20M-HA}$ and *Cfap410*$^{HA/R73P-HA}$ neuronal cultures in comparison to control (~6-9%, $P<0.05$, Figure 6f-h). The nuclear to cytoplasmic redistribution was more frequently observed in homozygous clones, particularly *Cfap410*$^{R73P-HA/R73P-HA}$ (13.5-14.2%, σ 2.4-4.9%) as compared to *Cfap410*$^{V20M-HA/V20M-HA}$ (8.7-6.4%, σ 1.5-3.8%). In a small number of cells, TDP43 was observed not only in the soma but also along the neurites (Figure 6f-h, white bars). This was particularly noticeable in cultures of *Cfap410* ALS homozygous variant neurons after ETO treatment where 2.7% (σ 1.6%) of neurons showed TDP43 localised in the soma and neurites in comparison to 0.9% (σ 0.6%) of control neurons.

Cfap410 ALS variant knock-in ESCs, NPCs and neurons are more susceptible to DNA damage.

Cfap410 has been implicated in the DNA damage response (DDR) and is seen to be associated with other DDR proteins such as NEK1 (Fang et al., 2015). Since we observed reduced interactions between Cfap410 ALS variants and Nek1 by co-IP, we examined how the DNA damage response was activated in response to stress upon treatment with ETO, VAL and ARS. Histone H2AX is phosphorylated on Ser-139 (γH2AX) and forms foci where double strand DNA breaks have occurred (Mah et al., 2010). We quantified γH2AX levels in response to drug treatment in control and *Cfap410* ALS variant knockin ESCs, NPCs and neuronal cultures to see the effects on the DNA damage response.

Immunostaining for both γH2AX and P53BP1 showed a low level of DDR in ESCs (Figure 7a) and NPCs (Figure 7b). Quantification showed no significant differences between all the untreated cell lines (Figure S8c-d). Treatment of ESCs with ETO (Figure 7a), VAL or ARS (Figure S7a) resulted in increased levels of γH2AX and P53BP1 in the nucleus in a genotype dependent manner. Quantification consistently showed that significantly more γH2AX was present in the nucleus of ESCs carrying either the *Cfap410*$^{V20M\text{-}HA/V20M\text{-}HA}$ or *Cfap410*$^{R73P\text{-}HA/R73P\text{-}HA}$ ALS variants ($P<0.05$, Figure7c-e). Of the heterozygous clones, only those with the genotype *Cfap410*$^{+/R73P\text{-}HA}$ showed significantly increased γH2AX levels in comparison to *Cfap410*$^{WT/WT}$ and $^{HA/HA}$. In the case of *Cfap410*$^{+/V20M\text{-}HA}$, only clone C13 was significantly different from the controls after ETO or ARS treatment but not upon treatment with VAL ($P<0.05$, Figure 7c-e).

A similar trend was observed in ETO, VAL or ARS treated NPCs (Figure 7f-h). However, here the *Cfap410*$^{+/R73P\text{-}HA}$ clones showed a reduced but still significant response in comparison to the equivalent ESC clones (Figure 7c-e). The heterozygous *Cfap410*$^{+/R73P\text{-}HA}$ clones were affected significantly when compared to the controls unlike the *Cfap410*$^{+/V20M\text{-}HA}$ when treated with ETO and VAL.

In untreated motor neuron cultures, minimal γH2AX levels were observed as was the case with ESC and NPC cultures (Figure S8a, quantified in Figure S8e). A trend of increased γH2AX levels in untreated homozygous *Cfap410* ALS variant neurons was observed but this did not appear to be significant ($P>0.05$) (Figure 8a, S8e). After treatment with ETO, γH2AX and P53BP1 levels were highest in *Cfap410*$^{V20M\text{-}HA/V20M\text{-}HA}$ and *Cfap410*$^{R73P\text{-}HA/R73P\text{-}HA}$ neurons (Figure 8a). Quantification of this after ETO treatment showed that neuronal cultures differentiated from two independent clones homozygous for either of the *Cfap410* ALS variants have γH2AX levels significantly higher than controls (Figure 8b, $P<0.005$). The same trends and significant differences in γH2AX levels were found in VAL (Figure 8c) and ARS treated neurons (Figure 8a, quantified in Figure 8d). With both VAL and ARS treatment, the responses observed in neurons differentiated from either sets of heterozygous clones (i.e. both clones of *Cfap410*$^{+/V20M\text{-}HA}$ and *Cfap410*$^{+/R73P\text{-}HA}$) were muted.

Western blots were performed to confirm the increased γH2AX and P53BP1 levels observed by immunofluorescence for ETO treated neurons (Figure 8e). Here, heterozygous clones were used to better represent the patient-associated genotype. Densitometry showed significantly higher amounts of γH2AX and P53BP1 present in *Cfap410* variant neurons after ETO treatment (Figure 8f). ETO is known to activate the ATR-CHK1 DDR pathway in neurons and other cell types so we examined whether the phosphorylation of CHK1 was also occurring here (Lu et al., 2002; Semple et al., 2007). Immunoblotting showed no changes in total CHK1 levels between WT and ALS variant *Cfap410* neurons (Figure 8e-f). Little to no phospho-CHK1 (pCHK1) could be detected in untreated neurons however levels were increased after ETO treatment in all cultures, though to a lesser degree in *Cfap410* ALS variant neurons (Figure 8f). When comparing between genotypes, the levels of phospho-CHK1 present in *Cfap410*$^{+/V20M\text{-}HA}$ and *Cfap410*$^{+/R73P\text{-}HA}$ appeared subdued.

Discussion

CFAP410 has been reported to be a component of the basal body of primary cilia and mutations in this protein have been found to be associated with ciliopathies (Thiel et al., 2011; Wheway et al.,2015, Wang et al., 2016, Khan et al., 2015, Schmidts et al., 2013). Primary cilia have been shown play an anti-apoptotic role in the central nervous system (Choi et al., 2019) and defects in primary cilia could lead to increased vulnerability of cells through multiple mechanisms such as inappropriate cell cycle re-entry, autophagy defects or the inability to transduce protective signalling (Choi et al., 2019; Ishii et al., 2020; Kaliszewski et al., 2015). Cfap410 has been shown to localize in ciliary structures of the photoreceptor cells (Schmidts et al., 2013). We found that in cells with HA tagged wild type and both the ALS variants knockin cells we studied, HA tagged Cfap410 localised to the basal body. However, we did not observe loss of cilia or any gross morphological effects on primary cilia in the neurons with the ALS variant knockins. It is possible that the two ALS variants we knocked into the Cfap410 gene may have caused subtle changes to the primary cilia. Further characterisation of primary cilia and basal body components or signalling pathways in the Cfap410 ALS variant knock in cells may identify more subtle defects if present.

Previous studies have demonstrated a role for CFAP410 and its interactor NEK1 in the DNA damage response (Chen et al., 2008; Fry et al., 2012; Wheway et al., 2015, Fang et al, 2015, Melo-Hanchuk et al., 2017) and an ALS associated variant in NEK1 shows increased DNA damage in motor neurons. We also found that ESCs, NPCs and MNs carrying the ALS knockin variants were more susceptible to DNA damage when subjected to genotoxic stress. However, we found that heterozygous cells with the V20M variant were less susceptible as compared to the R73P variant.

In the V20M *Cfap410* variant the residue change is from a hydrophobic to polar one and in addition there is a change from a shorter side chain to a longer one. Since V20 is conserved across species, we previously predicted that there is likely to be phenotypic consequences of this change (Iyer et al 2018) which we do see in the form of increased susceptibility to DNA damage.

The R73P variant of *Cfap410* has been implicated in a ciliopathy-Axial spondylometaphyseal dysplasia as reported by Wang et al (2016). The effect of the R73 to P change is quite severe as proline is a non-polar residue whilst arginine is positively charged. We had predicted that in addition, the change from arginine to proline will cause conformational rigidity in the protein chain leading to a significant effect on the local protein structure around the site of mutation thus leading to functional effects (Iyer et al, 2018). Our data shows that this is indeed the case as we do see a more severe effect on the susceptibility to DNA damage in both heterozygous and homozygous R73P variant knockin cells.

In one recent study the V58L CFAP410 (C21ORF2) ALS variant was reported to be more stable than the wildtype protein due to increased phosphorylation by NEK1 and it was suggested that an accumulation of both NEK1 and CFAP410 (C21ORF2) leads to an aberrant phenotype in motor neurons (Watanabe et al, 2020). Our ALS variant knock in neurons showed a trend towards a reduction in the interaction with Nek1 as well as other interactors such as SpatA7.

In addition, we also found that the DNA damage response (DDR) is affected in the *Cfap410* ALS variant knock in cells. Checkpoint kinase 1 (Chk1), an important mediator and signal transducer in DDR (Dai and Grant, 2010) is activated by phosphorylation. We found that this happens to a lesser extent in the ALS variant knockin neurons resulting in an attenuation of the activation of DNA damage checkpoints possibly leading to aberrant activation of DNA repair pathways (Harper and Elledge, 2007; Chen and Poon, 2008; Blasius et al, 201). It is known that activated Chk1 phosphorylates Cell division cycle 25 (Cdc25) leading to cell cycle arrest (Sanchez et al, 1997). Regulation of Cdc25B by Chk1 appears to occur at centrosomes. Phosphorylation of Cdc25B by Chk1 results in its sequestration from the centrosome leading to inhibition of centrosomal cyclin-dependent kinase 1 (Cdk1; Kramer et al, 2004). Since Cfap410 is a basalbody/centrosomal protein, mutations in this protein may affect the localization of Cdcs. Further studies along these lines will shed light on the possible mechanisms by which Cfap410 variants cause ALS. DNA damage and repair appears to be a major pathway that is affected in neurodegenerative disorders (Abugable et al, 2019; Pessina et al, 2021).

Methods

Cell culture

R1 mouse embryonic stem cells (R1 mESCs) were cultured on 0.1% gelatin (porcine skin gelatin, Sigma) coated tissue culture dishes (Falcon) in DMEM (Gibco Life Technologies) supplemented with 10% Knockout serum replacement (GibcoLife Technologies), 5% FBS (Labtech), 10 ng/mL Leukemia inhibitory factor (LIF) , 1 % non-essential amino acid (NEAA; Gibco), 1μM PD-0325901 (Tocris), 3μM CHIR99021 (Cayman), 0.1 mM β-mercaptoethanol (Sigma). R1mESCs were sub-cultured every two days using 0.05% trypsin EDTA (Gibco Life Technologies). P19 embryonal carcinoma cells (McBurney and Rogers, 1982) were cultured in α-MEM (Gibco Life Technologies) supplemented with 10% FBS (Biosera) and 1% NEAA on gelatin coated tissue culture dishes. Media was changed every day and cells were subcultured every two days using 0.05% trypsin EDTA. Neural progenitor cells (NPCs) for expansion were maintained

on Matrigel (Corning) coated dishes in DMEM:F12 (Gibco Life Technologies) supplemented with 1x B27 (Gibco Life Technologies), 20ng/ml EGF, 20ng/ml FGF (both from Peprotech). All cell cultures were maintained at 37°C in 5% CO2.

Differentiation of P19 cells

Cells were washed with PBS and trypsinised with 0.05% Trypsin EDTA (Gibco Life Technologies). $2.5x10^5$ cells/ml were seeded in 90mm suspension dishes (Sterilin) in a-MEM supplemented with 10% KOSR (Gibco Life Technologies), 1% Glutamax and 1% NEAA. Retinoic acid (0.5 μM; Sigma) was added after 24h. After 48h, EBs were plated onto Matrigel (BD)-coated coverslips in a-MEM, 1% Glutamax, 1% NEAA, 1% KOSR and 0.5 μM retinoic acid. This media was changed every other day until day six when it was changed to neurobasal media containing 1x B27 (Gibco Life Technologies), 1% KOSR and 1% Glutamax.

Isolation of mouse brain tissue

Pregnant C57BL/6J dams were killed by cervical dislocation prior to dissection for isolating brains from embryonic stages. E18.5 brains were split into fore and mid-brain. Postnatal brains were split into cerebrum and cerebellum. Tissues were snap frozen in Trizol (1ml per 50mg), freeze thawed and disrupted using a Dounce homogeniser.

RNA isolation and cDNA synthesis

P19 cells for RT-qPCR were harvested at appropriate time points on differentiation . (MacPherson and McBurney, 1995) modified as in Ferguson et al., 2016. Adherent cells were lysed in 1ml/cm2 Trizol (Invitrogen), scraped, transferred to a centrifuge tube and briefly vortexed to fully lyse the cells. RNA was isolated from the Trizol lysates following manufacturer's instructions. RNA yield was determined using Nanodrop spectrophotometer and RNA quality assessed on 1.5% denaturing agarose gel. Equal masses of RNA were re-precipitated and dissolved in equal volumes of DEPC (Sigma) water then treated with RNAse free DNAse (Ambion) at 37°C for 30 min. Quantity and quality were checked again as before. Total RNA was annealed to oligo-dT primers. cDNA synthesis was performed using M-MuLV H-minus reverse transcriptase for one hour at 42°C and inactivated at 70°C for five minutes (all components from RevertAid™ H Minus Reverse Transcriptase kit, Fermentas). Duplicate reactions substituting the RT enzyme for DEPC treated water were also performed as above for each sample. RT reactions were performed at 42°C for 60min and inactivated by 5min at 70°C. Each reaction was diluted to 10ng/ul of starting material in H2O.

Quantitative PCR

A Mastermix comprising iQ SYBR Green supermix (BioRad), water and cDNA was made for quantitative PCR. Appropriate primers were added and divided into three replicates for each gene on PCR plates (Thermo). Final reactions were 20µl in volume with 0.1µM primers and 10ng cDNA (see Supplementary Table 1 for primer sequences). Reactions were performed in a BioRad iQ5 cycler. Dynamic well factors were collected for 2min 30sec, then forty cycles at 60°C and 95°C for 20s each followed by a melt curve. Expression levels were determined relative to GAPDH from baseline subtracted curves and corrected using primer efficiencies determined previously from serial dilutions of PCR product. qPCR reactions were conducted in triplicate in three independent experiments.

Guide design and cloning

Using the mouse *CFAP410* locus (GRCm38 10 7797802-77987405). Guide pairs were designed using chopchop.cbu.uib.no and crispr.mit.edu. See main text for rationale. For each edit site, four pairs of guides which showed no joint off-target binding and were proximal to the desired insert site were chosen. See Table 2. Oligos encoding the guide sequences were designed to include overhangs compatible with the multiplex pX330 based nickase Cas9 constructs (gift from T Yamomoto; Sakuma et al., 2014). The oligos comprising each pair of guides were hybridised by cooling from 95□ cloned by Golden Gate assembly into the BbsI sites of either pX330A1x2 (sgRNA-A) or pX330S-2 (sgRNA-B) using T4 ligase (Thermo). Were transformed into DH5a. Colonies were screened by colony PCR. Positive clones were confirmed by sequencing from the U6 promoter (Eurofins MWG U6 primer). The sgRNA-B expression cassette from pX330S-2 was transferred into the BsaI sites of the corresponding pX330A1x2 sgRNA-A plasmid again by Golden Gate assembly. Clones were screened by NdeI digest.

Cloning of Heterozygous alleles for sequencing

Purified Q5 PCR products from potential heterozygous clones to be further characterised were ligated into SmaI digested pBluescript II KS (+) (100ng) in 20µl 1:3 reactions with 1x T4 ligase buffer (Thermo), 5U T4 ligase (Thermo), 10U SmaI (Thermo). Reactions were run on PCR machine with the following cycling parameters: 10x 20min@25^{o}C, 30x 1min@10^{o}C, 30s@22^{o}C 30s@4^{o}C, 30s@30^{o}C, 1h@25^{o}C then held at 4^{o}C (Pusch et al., 1997). Ligations were transformed into DH10B (NEB), and clones analysed by colony PCR using GoTaq G2 Flexi (Promega) in 30µl reactions comprised of 1x 'Green' Flexi buffer (Promega), 1.5mM MgCl2, 0.2mM dNTPs (Bioline), 0.5µM of C21_R361Q_HA_F2/R2 and 0.025U GoTaq G2 polymerase. PCRs were performed using the following protocol: 98□C for 2min, then thirty cycles of 98□C for 20s, annealing for 20s and extension at 72□C (see supplementary table 1 for details), followed

by a final extension at 72□C for 5min. Completed reactions were digested in 50ul with 1x EcoRI buffer and 0.5U EcoRI (Thermo) for 1h at 37□. Variant clones from each transformation were analysed by sequencing using the T7 promoter.

Cloning of genomic donor targeting vectors

To create the donor plasmid backbone pBS-puDtk, the PGK Puro-deltaTK cassette of pPB-CAG.OSKML-puDtk (gift from A Bradley; Yusa et al., 2009) was amplified by PCR using Q5 HiFi polymerase (NEB) and primers containing SapI sites with variable overhang homologous to that of the SapI site of pBluescript II KS (+) (See supplementary table 3 for sequences). PCR products and pBluescript were digested with SapI, gel purified and ligated using T4 ligase (Thermo) and transformed into DH10b.

Homology arms derived by PCR from the BAC clone bMQ207-G4 from the 129S7/AB2.2 BAC library (Source Bioscience). The intended mutation or epitope tag, a novel synonymous restriction site and a mutated PAM site were included in overlapping central primers while outer primers were appended with the sequences flanking the EcoRV site of pBS-puDtk. See primers listed in supplementary table 3. The PCR cycling parameters used were 1x Q5 (NEB), 0.5μM of forward and reverse primer and 5ng of BAC in a 50μl reaction. PCR products and EcoRV linearised pBS-puDtk were purified by gel excision and assembled in a 20μl reaction with 50ng of vector and 100ng of each homology arm fragment and 1x HiFi DNA Assembly mix (NEB). Reactions were transformed in NEB Stable cells.

Correct assembly was confirmed by sequencing using the T7 and M13 promoter primers (stock primers, Eurofin MWG) and across the central join using primers upstream of the HA, V20M and R73P donors respectively.

Screening of Guides

R1 mESCs cultures at 70-80% confluency were fed with fresh media two hours prior to transfection. Single cell suspensions of R1 mESCs were transfected following the method of Tamm et al., (2016). pX330A1x2 nCas9 containing the guide pairs to be screened was used at 0.5ug per replicate on a 24well plate. DNA was complexed with Lipofectamine 2000 (Invitrogen) in OptiMEM (Gibco) at a ratio of 1:4 (Reagent:DNA) for 50μl per replicate. Cells were trypsinised to single cells, resuspended in complete medium and counted by haemocytometer. The appropriate numbers of cells in suspension was centrifuged at 270g for five minutes, resuspended in OptiMEM and centrifuged again. The final pellet was resuspended in OptiMEM to a final concentration of 10^5 cells per 50μl OptiMEM and mixed with 50μl DNA Lipofectamine solution and incubated at room temperature for five minutes. Cells were co-transfected with pCagTag (Gift from S Srinivas) Trichas et al., 2008) to determine transfection efficiency. The transfected cell suspension was transferred to pre-warmed media on gelatinised 24well plates with 500μl

complete medium per well. Transfected cells were analysed after 24h. Transfection efficiency was determined by fixing two wells for each primer pair with 4% PFA for ten minutes at room temperature, cells were counterstained with DAPI and the proportion of GFP expressing cells quantified from four different fields per condition. For determining sgRNA efficacy, duplicate wells were lysed for DNA extraction by proteinase K based methods.

Isolation of genomic DNA isolation from mammalian cells

DNA was prepared using either the HotShot method (Truett et al., 2000) or by lysis in Proteinase K (Roche) containing buffer followed by phenol:chloroform extraction as indicated For HotShot method, media was aspirated and cells were washed with PBS before adding 150µl/cm2 of lysis buffer (25 mM NaOH, 0.2 mM EDTA, both Sigma). Samples were incubated at 95□C for 15min then cooled briefly on ice before adding equal volume of neutralising buffer (40mM Tris-HCl, Sigma).

For proteinase K based DNA isolation, media was aspirated and cells were washed with PBS before adding 150µl/cm2 of lysis buffer (0.2 mg/ml proteinase K (Roche), 100mM NaCl, 0.5M EDTA, 0.5% SDS in 10mM Tris pH 8.0, all Sigma). After incubation overnight at 50□C lysates were transferred to microfuge tubes with equal volumes of phenol:chloroform:isoamyl alcohol (PCI, 25:24:1, MP biomedical, Sigma, Sigma). After mixing and centrifuging for five minutes at 16,000g, the aqueous phase was recovered and precipitated with 0.2M NaCl (final) and 75% ethanol (final). Precipitated DNA was pelleted at 16,000g for 15min, the supernatant discarded and replaced with 70% ethanol. After a further 10min centrifugation, the supernatant was discarded again and the pellet dried. DNA was dissolved in 200µl/cm2 TE (1mM EDTA in 10mM Tris pH 8.0, both Sigma).

T7E1 assay

The fraction of modifications introduced by CRISPR/Cas9 to the targeted site was determined by T7 endonuclease 1 digestion of the resulting heteroduplexes formed after PCR and subsequent rehybridisation (Mashal et al., 1995). Primers to amplify asymmetrically across the intended edit point were designed and optimised by gradient PCR using Q5 high fidelity Taq mix (NEB). PCRs were performed using 10ng of DNA prepared by proteinase K and PCI extraction in 50µl with 0.5µM primers. PCR conditions were 95□C for 2min followed by thirty cycles of 95□C 10s, Ta 10s, 72□C 20s, 72□C 5min then 10□C hold See supplementary table 1 for annealing temperatures and primer sequences. PCR products were purified by spin column (QIAquick PCR Purification Kit, Qiagen) and eluted in sterile water. 200ng of the PCR product was diluted in NEB buffer 2 and rehybridised by heating to 95□C for five minutes then lowering the temperature from 95-85□C at -2□C/s then 85-25□C at -0.1□C/s. 10U of T7E1 (NEB) or water (as control) was added to each reaction to bring the final volume to 20µl and the reactions incubated at 37 for 15 min. EDTA was added to a final concentration of 25mM to stop the reaction. Reactions were

electrophoresed on 2% TBE agarose gels and band intensity quantified using ImageJ. Gene edited fractions were calculated as % gene modification = 100 × (1 − (1 − fraction cleaved)1/2) from three independent experiments.

Electroporation of ES cells

R1 mESCs were washed with PBS and trypsinised to single cells, resuspended in complete medium and counted using a haemocytometer.

For electroporations using the Bio-Rad genepulser, $5x10^6$ cell were centrifuged at 270g for 5min, resuspended in PBS and centrifuged again. Cells were resuspended in 800µl of PBS containing 25µg of the pBS PuroDtk donor plasmid, 2.5µg pX330A containing the corresponding opitimal guide pair and 2.5µg pDisplay mSA EGFP TM (gift from Sheldon Park, Addgene plasmid 39863). The suspension was then transferred to 1ml 2mm path cuvettes (Biorad) and electroporated at 300V, 250µF.

For electroporations using the NEPA21 electroporator (Nepagene), $1x10^6$ cell were centrifuged at 270g for 5min, resuspended in PBS and centrifuged again then resuspended in OptiMEM (Gibco) and centrifuged again. Cells were finally resuspended in 100µl of OptiMEM containing 10µg of the pBS PuroDtk donor plasmid , 2.5µg pX330A containing the corresponding guide pair and 2.5µg pDisplay mSA EGFP TM (Lim et al., 2013). The suspension was then transferred to 1ml 2mm path cuvettes (Nepagene) and electroporated using two poring pulses (+) at 135V for 5ms with 50ms intervals and a 10% decay rate followed by five transfer pulses (±) at 20V for 50ms with 50ms intervals with a 40% decay rate.

Electroporated cells were diluted 1:100 in complete ES medium medium and seeded at $1ml/10cm^2$. 18h after electroporation, media was changed to include 0.5µg/ml puromycin (Sigma). Selection was maintained for 48h after which magnetic sorting was performed. Anti-HA beads (Pierce) were washed in and kept in PBS with 0.1% BSA (PBS-BSA). Cells were trypsinised and centrifuged at 270g for 5min, resuspended in PBS-BSA and spun down again. The cell pellet was resuspended in the 1ml of HA-bead suspension and incubated rocking for five minutes. The beads were pelleted by magnet for one minute after which the supernatant was aspirated and the pellet resuspended in PBS-BSA. This was repeated once more and the pellet resuspended in complete medium. Sorted cells were seeded at a density of 750 cells per 10cm2 on gelatinised dishes in complete medium. Only 50% media changes were made after 24-36h until colonies had established. Once large enough, colonies were picked to individual wells of a 24 well plate and expanded for characterisation.

High resolution melt curve analysis

PCRs were performed on 50ng of genomic DNA isolated form individual ES clones using GoTaq G2 Flexi (Promega) in 50µl reactions containing 1x colourless GoTaq reaction buffer, 0.2mM dNTPs (Bioline),

0.75U GoTaq polymerase, 0.5x EvaGreen (Biotium), assay dependent concentrations of $MgCl_2$ (1.0μM and 1.2μM for V20M and R73P, respectively) and primers (See Table S1 for primer sequences). PCR cycling conditions were 3min at 95□C followed by 30 cycles of 95□C for 15s, T_a for 15s and 72□C for 20s then a final extension at 72□C for 5min (See Table 1 for T_a). Where digestion of the PCR product was performed, reactions were divided in two aliquots and 0.5U of Tru1I (MseI) (Thermo) added in 10μl reaction volume containing 1x Buffer R. Digests were incubated at 65□C for 1h. Melt curves were performed on a Biorad iQ5 with 0.1□C increments and 15s dwell time.

Differentiation of mouse ES cells

mESCs were trypsinised at 60-70% confluence, resuspended in the appropriate complete medium (ESC or NPC) and counted by haemocytometer. Cells well diluted to 10^5 cells/ml in DMEM:F12 with 10% KOSR, 1μM DMH1 (Tocris), 1μM SB (Tocris), 1% GlutaMax and 0.1 mM β-mercaptoethanol (Sigma), and plated in suspension in non-TC treated 10cm dishes (Sterilin) to form aggregates. Media was changed on day two. On day four, aggregates were collected in centrifuge tubes washed with PBS and disassociated using Accutase (Gibco; 3ml/10cm) for 30min at 37°C. NPC medium [DMEM:F12 (Gibco) supplemented with 1x B27 (Gibco), 20ng/ml EGF and 20ng/ml FGF] was added and cells were centrifuged at 270g for 3 minutes. After aspirating the supernatant, the pellets were resuspended in NPC medium, gently triturated, and counted by haemocytometer. They were then replated onto Matrigel coated dishes at a density of 104 cells/cm2 in NPC medium. After 72h of culture the NPCs were passaged using Accutase as before but with only a 3 minute incubation. NPCs were either expanded for characterisation or progressed to motor neuron differentiation. For motor neuron differentiation, media was changed 24h after passaging of NPC in DMEM:F12 supplemented with 1x B27, 1x GlutaMax, 1μM Retinoic acid (Sigma), 1μM Purmorphamine (Tocris) and 20ng/ml BDNF, GDNF and CNTF (all Peprotech). After a further 48h culture, neurons were washed with PBS and incubated for 30min with Accutase. Neurons were resuspended in MN medium, centrifuged at 270g for 3 minutes. After aspirating the supernatant, the pellets were resuspended in MN medium, gently triturated, and counted by haemocytometer. They were then replated onto poly-l-ornithine and laminin (both Sigma) coated dishes or coverslips at a density of 10^5 cells/cm^2 in MN medium.

Colony forming assays

Cells were trypsinised at 60-70% confluency, resuspended in the appropriate complete medium (ESC or NPC) and counted by haemocytometer. For ESCs, 2ml of medium was pre-warmed on gelatin coated 12well plates (Falcon). Cells were diluted to 1500 cells/ml and 100μl dispensed to the 12 well plates for a final concentration of 150 cells per well in triplicate. Media was changed after 48h, then every 24h until the fifth day. For NPCs, non-TC treated 12well plates (Falcon) were coated with 0.5% agar (in 1x

DMEM:F12). 2x stocks of agar and DMEM:F12 were made and autoclaved or sterile filtered respectively before combining for use. 2x NPC medium was combined with 0.6% agar for final concentrations of 0.3% agar, 20ng/ml EGF (Peprotech), 20ng/ml FGF (Peprotech), 1x B27 (Gibco), 1x GlutaMax (Gibco), 1x DMEM:F12 (Gibco) and kept at 40□C in a water bath. Cells were diluted to 1500 cells/ml and 100µl dispensed to the 12 well plates for a final concentration of 150 cells per well in triplicate. 1ml of agar media was added to each well gently mixed by pipette and allowed to cool at room temperature for 20min. 1ml of complete medium was added on top before returning to the cell culture incubator. Media was changed every 48h for eight days.

The colonies formed after 8 days of culture were washed with PBS, fixed in 4% PFA for 30min RT and stained with 0.01% crystal violet (BDH) for 30min. Stained cells were washed with water until the background was clear. Plates were imaged on a UVP Gel-doc IT2 Imager and colony frequency and area were measured using Fiji. Data was collected from three replicates from three independent experiments.

Growth assays

Cells were trypsinised at 60-70% confluence, resuspended in the appropriate complete medium (ESC or NPC) and counted by haemocytometer. Cells were diluted to $3.2x10^4$ cells/ml in complete medium. 100µl per well of cell suspension was plated in triplicate for each cell line for each assay interval on 96 well plates for $1x10^4$cells/cm^2. Growth was assayed using the Non-Radioactive Cell Proliferation Assay (Promega) at 24h intervals. Cells were incubated with 15µl/well of dye solution for 2h followed by 100µl of stop solution. After solubilisation for 1h, absorbance was recorded at 570nm with a 700nm reference wavelength.

Kill curve assays

Cells were treated with varying concentrations of Etoposide (MP Biomedical), Valinomycin (Sigma) and Sodium Arsenite (BDH). Cells were trypsinised at 60-70% confluence, resuspended in the appropriate complete medium (ESC or NPC) and counted by haemocytometer. Cells were diluted to 19.2 x 10^4 cells/ml in complete medium. Cell suspension (50µl per well) was plated in triplicate for each cell line on 96 well plates for $3x10^4$cells/cm^2. A dilution series of the appropriate drug in solvent was created such that each was added to complete medium for a final solvent concentration of 0.1% (DMSO) across the series. Drugs were diluted to 2x the indicated concentration in complete medium and added as 50µl per well for the final 1x concentration. Concentrations used were a 1:3 series from 100-0.14µM for etoposide and valinomycin, and 30.0-0.04 µM for sodium arsenite. Viability was determined after 24h using the Non-Radioactive Cell Proliferation Assay (Promega), as described in ‘Growth assays’.

Drug treatment of EC, NPCs and Motor neurons

ESC and NPC were plated at $3x10^4$cells/cm^2 as described above. Neuronal cultures were differentiated as described and replated at a density of 10^5 cells/cm^2 in MN medium onto poly-l-ornithine and laminin (both Sigma) coated coverslips for immunostaining, or coated T75s for protein lysates. Etoposide, valinomycin and sodium arsenite concentrations used represent the [EC50] for the heterozygous V20M genotype for each cell type. Neurons: 2μM etoposide, 0.5μM sodium arsenite, 2μM Valinomycin. After 16h treatment, cells were fixed for immunostaining, or lysed for Co-IP/Western blot.

Western blot

Cells were lysed in RIPA buffer (50mM Tris pH7.4, 150mM NaCl, 1% NP40, 0.5% sodium deoxycholate, 0.1% SDS, 1mM EDTA, 1mM PMSF) with 1x cOmplete Mini Protease Inhibitors (Roche). Protein concentration was determined using the BCA assay (Pierce).

For blotting, 50μg of lysate were run on a 12% tris-tricine gel (Haider et al., 2012; Schägger, 2006). Proteins were transferred to 0.22μm PVDF (Millipore) at 50V for 4h in transfer buffer 25mM Tris, 192mM glycine, pH 8.3, 20% methanol. Membranes were blocked in 5% milk (Marvel) in PBS with 0.1% Tween (PBSTw) for one hour and incubated overnight at 4°C with primary antibodies diluted in block. Blots were washed four times for ten minutes each in PBSTw before incubation with Horseradish peroxidase (HRP) conjugated secondary antibodies for one hour at RT. See supplementary table 4 for antibody dilutions. After a further four ten minute PBSTw washes and two PBS washes, blots were incubated with lab made ECL reagent (Haan and Behrmann, 2007) and imaged on a Fusion SL (Vilber Lourmat).

Immunoprecipitation

Cells were lysed in 100μl/cm2 of buffer comprised of 20mM Tris (pH7.5) with 150mM NaCl, 1mM EDTA, 1mM EGTA, 1% Triton X-100, 1mM PMSF (all Sigma) and 1x cOmplete Mini EDTA-free Protease Inhibitor Cocktail (Roche). All steps were done on ice or 4°C with precooled material. Cells were scraped to collect and rocked for 30min before centrifugation at 10,000g for 20min. The supernatant was recovered and protein concentration estimated by BCA assay (Pierce). 2mg of lysate was incubated overnight on a rotator with 50μg Anti-HA magnetic beads (Pierce). Beads were washed three times with PBSTw and eluted twice with 20μl Laemmli buffer and pooled.

Immunostaining

Cells cultured on coverslips were washed with PBS and fixed for 15min in 4% PFA. PFA was washed off with two PBS washes and cells dehydrated to 70% ethanol through 30% and 50% for ten minutes each. After rehydration to PBS, wells were incubated in block for 1h RT (PBS with 1% FBS, 0.1% gelatin and 0.5% Triton X-100). Incubation with primary antibody in PBST (PBS with 0.1% Tween) with 0.1% FBS was performed overnight at 4□C. After four PBST washes for ten minutes each, cells were incubated with secondary antibodies together 4',6-diamidino-2-phenylindole (DAPI, Sigma). See supplementary table 4 for antibody dilutions. Z-stacked images were acquired with either a Leica DM5500B microscope, DFC 360FX camera and LAS software and deconvoluted or using a Zeiss LSM510META confocal microscope using LSM 5 Series software.

Quantification of nuclear phospho-YH2AX levels

Images were acquired as 3D stacks from four random positions for each condition from three independent experiments. Stacks were deconvoluted in LAS AF. Deconvoluted stacks were subjected to flat-field correction using BaSiC in Fiji, followed by maximum intensity projection. Nuclear masks were created using the DAPI channel. Median grey values for each nuclei were measured for the channel to be quantified.

Statistical Methods

Each experiment was repeated at least three times using at least two independent cell lines of the same genotype. Images were acquired from at least five random fields in each experiment. Images for quantification were acquired at equal gain and exposure, flat field corrected using the BaSiC ImageJ plugin (Peng et al., 2017) and further analysed using Fiji as described in the detailed methods. Where possible datapoints representing the quantification of result from each independent experiment are presented dots plotted over bar graphs showing overall mean ±SEM. Where fluorescent intensity analyses have been performed, plots based on median single cell fluorescent intensity are presented. See figure legends for more specific details. Normality was determined using the D'Agostino-Pearson test. Normal data was tested directly using ANOVA and Bonferroni post-hoc. Statistical analysis was performed using either SPSS 23 or R.

References

Abugable, A.A., Morris, J.L.M., Palminha, N.M., Zaksauskaite, R., Ray, S. and El-Khamisy, S.F. (2019) DNA repair and neurological disease: From molecular understanding to the development of diagnostics and model organisms. DNA Repair (Amst). 81:102669.

Bai, S.W., Herrera-Abreu, M.T., et al.,. (2011) Identification and characterization of a set of conserved and new regulators of cytoskeletal organization, cell morphology and migration BMC Biology, 9, 54.

Blasius M, Forment JV, Thakkar N, Wagner SA, Choudhary C, Jackson SP. A phospho-proteomicscreen identifies substrates of the checkpoint kinase Chk1. Genome Biol. 2011; 12:R78.

Brenner, D., Muller, K., Wieland, T., Weydt, P., Bohm, S., Lule, D., Hubers, A., Neuwirth, C.,Weber, M., Borck, G., et al. (2016). NEK1 mutations in familial amyotrophic lateral sclerosis. Brain. 139, e28.

Brown, R.H., and Al-Chalabi, A. (2017). Amyotrophic Lateral Sclerosis. N. Engl. J. Med. 377, 162–172.

Chia, R., Chio, A., and Traynor, B.J. (2018). Novel genes associated with amyotrophic lateral sclerosis: diagnostic and clinical implications. Lancet Neurol. 17, 94–102.

Chen, Y., Chen, P.L., Chen, C.F., Jiang, X., and Riley, D.J. (2008). Never-in-mitosis related kinase1 functions in DNA damage response and checkpoint control. Cell Cycle 7, 3194–3201.

Chen Y, Poon RY. The multiple checkpoint functions of CHK1 and CHK2 in maintenance ofgenome stability. Front Biosci. 2008; 13:5016–5029.

Chiò A, Logroscino G, Traynor BJ, et al. Global epidemiology of amyotrophic lateral sclerosis: a systematic review of the published literature. Neuroepidemiology. 2013;41:118-130

Choi, B.K.A., D'Onofrio, P.M., Shabanzadeh, A.P., and Koeberle, P.D. (2019). Stabilization of primary cilia reduces abortive cell cycle re-entry to protect injured adult CNS neurons from apoptosis. PLOS ONE *14*, e0220056.

Cirulli, E.T., Lasseigne, B.N., Petrovski, S., Sapp, P.C., Dion, P.A., Leblond, C.S., Couthouis, J., Lu,Y.F., Wang, Q., Krueger, B.J., et al. (2015). Exome sequencing in amyotrophic lateral sclerosis identifies risk genes and pathways. Science 347, 1436–1441.

Dai Y, Grant S. New insights into checkpoint kinase 1 in the DNA damage response signaling network. Clin Cancer Res. 2010; 16:376–383.

Fang, X., Lin, H., Wang, X., Zuo, Q., Qin, J., and Zhang, P. (2015). The NEK1 interactor, C21ORF2, is required for efficient DNA damage repair. Acta Biochim. Biophys. Sin. *47*, 834–841.

Fliegauf, M., Benzing, T., and Omran, H. (2007). When cilia go bad: cilia defects and ciliopathies. Nat. Rev. Mol. Cell Biol. 8, 880–893.

Fry, A.M., O'Regan, L., Sabir, S.R., and Bayliss, R. (2012). Cell cycle regulation by the NEK family of protein kinases. J. Cell Sci. 125, 4423–4433.

Gratten, J., Zhao, Q., Benyamin, B., Garton, F., He, J., Leo, P.J., Mangelsdorf, M., Anderson, L.,Zhang, Z.H., Chen, L., et al. (2017). Whole-exome sequencing in amyotrophic lateral sclerosis suggests NEK1 is a risk gene in Chinese. Genome Med. 9, 97.

Haan, C. and Behrmann, I. (2007) A Cost Effective Non-Commercial ECL-Solution for Western Blot Detections Yielding Strong Signals and Low Background. Journal of Immunological Methods, 318, 11-19.

Harper, J. W. and Elledge, S.J. The DNA damage response: ten years after. Mol Cell. 2007; 28:739–745.

Hu, Y., Li, J., Lou, B., Wu, R., Wang, G., Lu, C., Wang, H., Pi, J., and Xu, Y. (2020). The Role of Reactive Oxygen Species in Arsenic Toxicity. Biomolecules *10*.

Haider, S.R., Reid, H. J., Sharp, B. L. (2012) Tricine-SDS-PAGE. Methods Mol Biol. 869:81-91

Hardiman, O., Ammar Al-Chalabi, Adriano Chio et al. (2017). Nature Reviews Disease Primers. 3, 17071.

Higelin, J., Catanese, A., Semelink-Sedlacek, L.L., Oeztuerk, S., Lutz, A.K., Bausinger, J., Barbi, G., Speit, G., Andersen, P.M., Ludolph, A.C., et al.(2018). NEK1 loss-of-function mutation induces DNA damage accumulation in ALS patient derived motoneurons. Stem Cell Res. 30, 150–162.

Huang, S., Liu, Y., Liu, W.-Q., Neubauer, P., and Li, J. (2021). The Nonribosomal Peptide Valinomycin: From Discovery to Bioactivity and Biosynthesis. Microorganisms *9*.

Ishii, S., Sasaki, T., Mohammad, S., Hwang, H., Tomy, E., Somaa, F., Ishibashi, N., Okano, H., Rakic, P., Hashimoto-Torii, K., et al. (2020). Primary cilia safeguard cortical neurons in neonatal mouse forebrain from environmental stress-induced dendritic degeneration. Proc. Natl. Acad. Sci. *118*.

Iyer S, Acharya, K. R,, Subramanian, V. (2019) Prediction of structural consequences for disease causing variants in C21orf2 protein using computational approaches. J Biomol Struct Dyn. 37:465-480

Jänicke, R.U., Sprengart, M.L., Wati, M.R., and Porter, A.G. (1998). Caspase-3 is required for DNA fragmentation and morphological changes associated with apoptosis. J. Biol. Chem. *273*, 9357–9360.

Kaliszewski, M., Knott, A.B., and Bossy-Wetzel, E. (2015). Primary cilia and autophagic dysfunction in Huntington's disease. Cell Death Differ. *22*, 1413–1424.

Kenna, K.P., van Doormaal, P.T., Dekker, A.M., Ticozzi, N., Kenna, B.J., Diekstra, F.P., van Rheenen, W., van Eijk, K.R., Jones, A.R., Keagle, P., et al. (2016). Nat. Genet. 48, 1037–1042.

Khan, A.O., Eisenberger, T., Nagel-Wolfrum, K., Wolfrum, U., and Bolz, H.J. (2015). C21orf2 is mutated in recessive early-onset retinal dystrophy with macular staphyloma and encodes a protein that localises to the photoreceptor primary cilium. Br. J. Ophthalmol. *99*, 1725–1731.

Kramer, A., Mailand, N., Lukas, C., Syljuasen, R.G, Wilkinson, C.J., Nigg, E. A., Bartek, J., and Lukas, J. Centrosome-associated Chk1 prevents premature activation of cyclin-B-Cdk1 kinase. Nat. Cell. Biol. 2004; 6:884–891.

Ling, S.C., Polymenidou, M., and Cleveland, D.W. (2013). Converging mechanisms in ALS and FTD:disrupted RNA and protein homeostasis. Neuron79, 416–438.

Lai, C.K. et al. Functional characterization of putative cilia genes by high-content analysis. Mol. Biol. Cell 22, 1104–1119 (2011).

Li, Y., Ling, K., and Hu, J. (2012). The emerging role of Arf/Arl Small GTPases in Cilia and Ciliopathies. J. Cell. Biochem. *113*, 2201–2207.

Lim, K.H., Huang, H., Pralle, A., and Park, S. (2013). Stable, high-affinity streptavidin monomer for protein labeling and monovalent biotin detection. Biotechnol. Bioeng. *110*, 57–67.

Lu, C., Fu, W., Zhao, D., and Mattson, M.P. (2002). The DNA damaging agent etoposide activates a cell survival pathway involving alpha-amino-3-hydroxy-5-methylisoxazole-4-propionate receptors and mitogen-activated protein kinases in hippocampal neurons. J. Neurosci. Res. *70*, 671–679.

Mah, L.-J., El-Osta, A., and Karagiannis, T.C. (2010). γH2AX: a sensitive molecular marker of DNA damage and repair. Leukemia *24*, 679–686.

Ma, X., Peterson, R., and Turnbull, J. (2011). Adenylyl cyclase type 3, a marker of primary cilia, is reduced in primary cell culture and in lumbar spinal cord in situ in G93A SOD1 mice. BMCNeurosci. 12, 71.

Mashal R. D., Koontz J., Sklar J. (1995) Detection of mutations by cleavage of DNA heteroduplexes with bacteriophage resolvases. *Nat. Genet.* 9: 177–183.

Melo-Hanchuk, T. D., Slepicka, P. F., Meirelles, G. V., Basei, F. L., Lovato, D. V., et al. (2017) NEK1 kinase domain structure and its dynamic protein interactome after exposure to Cisplatin. Sci Rep. 7:5445

Mejzini, R., Flynn, L. L, Pitout, I.L., Fletcher, S., Wilton, S.D. and P. Akkari, P. A. (2019) ALS Genetics, Mechanisms, and Therapeutics: Where Are We Now? Front Neurosci. 13: 1310.

Pelegrini, A.L. et al. Nek1 silencing slows down DNA repair and blocks DNA damage-induced cell cycle arrest. Mutagenesis 25, 447–454 (2010).

Peng, T., Thorn, K., Schroeder, T., Wang, L., et al. (2017). A BaSiC tool for background and shading correction of optical microscopy images. Nat. Comm. 8, 14836.

Pessina F, Gioia U, Brandi O, Farina S, Ceccon M, Francia S, d'Adda di Fagagna F. (2021) DNA Damage Triggers a New Phase in Neurodegeneration. Trends Genet. 37:337-354

Pusch, O., Bernaschek, G., Eilers, M.*et al.* (1997) Activation of c-Myc uncouples DNA replication from activation of G1-cyclin-dependent kinases. *Oncogene* **15,** 649–656 (1997)

Sakuma, T., Nishikawa, A., Kume, S., Chayama, K., & Yamamoto, T. (2014). Multiplex genome engineering in human cells using all-in-one CRISPR/Cas9 vector system. Scientific reports, *4*, 5400.

Sanchez, Y, Wong, C., Thoma R. S., Richman, R, Wu, Z., Piwnica-worms, H. and Elledge, S. J. Conservationof the Chk1 checkpoint pathway in mammals: linkage of DNA damage to Cdk regulation

through Cdc25. Science. 1997; 277:1497–1501

Schneider, C.A., Rasband, W.S., and Eliceiri, K.W. (2012). NIH Image to ImageJ: 25 years of image analysis. Nat Methods 9, 671-675.

Scott, H.S., Kyriakou, D.S., Peterson, P., Heino, M., Tahtinen, M., Krohn, K., Chen, H., Rossier, C.,Lalioti, M.D., and Antonarakis, S.E. (1998). Characterization of a novel gene, C21orf2, on human chromosome 21q22.3 and its exclusion as the APECED gene by mutation analysis. Genomics 47, 64–70.

Semple, J.I., Smits, V. a. J., Fernaud, J.-R., Mamely, I., and Freire, R. (2007). Cleavage and degradation of Claspin during apoptosis by caspases and the proteasome. Cell Death Differ. *14*, 1433–1442.

Schmidts, M., Arts, H. H., Bongers, E. M., Yap, Z., Oud, M. M.,et al. (2013) Exome sequencing identifies DYNC2H1 mutations as a common cause of asphyxiating thoracic dystrophy (Jeune syndrome) without major polydactyly, renal or retinal involvement. J. Med. Genet. 50: 309.

Schägger, H. (2006) Tricine-SDS-PAGE. Nature Protocols, 1, 16-22.

Shalom, O., Shalva, N., Altschuler, Y. & Motro, B. The mammalian Nek1 kinase is involved in primary cilium formation. FEBS Lett. 582, 1465–1470 (2008).

Suk, T.R., and Rousseaux, M.W.C. (2020). The role of TDP-43 mislocalization in amyotrophic lateral sclerosis. Mol. Neurodegener. *15*, 45.

Suga, A., Mizota, A., Kato, M., Kuniyoshi, K., Yoshitake, K., Sultan, W., Yamazaki, M., Shimomura, Y., Ikeo, K., Tsunoda, K., Iwata, T. (2016) Identification of novel mutations in the LRR-cap domain of C21orf2 in Japanese patients with retinitis pigmentosa and cone-rod dystrophy. Invest. Ophthal. Vis. Sci. 57: 4255-4263.

Tammaro, M., Barr, P., Ricci, B., and Yan, H. (2013). Replication-Dependent and Transcription-Dependent Mechanisms of DNA Double-Strand Break Induction by the Topoisomerase 2-Targeting Drug Etoposide. PLOS ONE *8*, e79202.

Thiel, C., Kessler, K., Giessl, A., Dimmler, A.,Shalev, S.A., von der Haar, S., Zenker, M.,Zahnleiter, D., Stoss, H., Beinder, E., et al. (2011). NEK1 mutations cause short-rib polydactylysyndrome type majewski. Am. J. Hum. Genet. 88, 106–114.

Thiyagarajan, N., Ferguson, R., Subramanian, V., and Acharya, K.R. (2012). Structural and molecular insights into the mechanism of action of human angiogenin-ALS variants in neurons. Nat. Commun. *3*, 1121.

Trichas, G., Begbie, J., and Srinivas, S. (2008). Use of the viral 2A peptide for bicistronic expression in transgenic mice. BMC Biol. *6*, 40.

Vouillot, L., Thélie, A., and Pollet, N. (2015). Comparison of T7E1 and surveyor mismatch cleavage assays to detect mutations triggered by engineered nucleases. G3 Bethesda Md *5*, 407–415.

van Rheenen, W., Shatunov, A., Dekker, A.M., McLaughlin, R.L., et al (2016) Genome-wide association analyses identify new risk variants and the genetic architecture of amyotrophic lateral sclerosis. Nature Genetics 48, 1043–1048.

Van Rheenen, W, Van der Spek, R.A.A. Bakker, M.K et al (2021). Common and rare variant association analyses in amyotrophic lateral sclerosis identify 15 risk loci with distinct genetic architectures and neuron-specific biology. Nature Genetics. 53, 1636–1648.

Wang, Z., Horemuzova, E., Iida, A., Guo, L., Liu, Y., Matsumoto, N., Nishimura, G., Nordgren, A., Miyake, N., Tham, E., et al. (2017). Axial spondylometaphyseal dysplasia is also caused by NEK1 mutations. J. Hum. Genet. 62, 503–506.

Wang, Z., Iida, A., Miyake, N., Nishiguchi, K.M.,Fujita, K., Nakazawa, T., Alswaid, A., Albalwi,M.A., Kim, O.H., Cho, T.J., et al. (2016). Axial spondylometaphyseal dysplasia is caused by C21orf2 mutations. PLoS One 11, e0150555.

Watanabe, Y., Nakagawa, T., Akiyama, T., Nakagawa, M., Suzuki, N., Warita, H., Aoki, M., and Nakayama, K. (2020). An Amyotrophic Lateral Sclerosis-Associated Mutant of C21ORF2 Is Stabilized by NEK1-Mediated Hyperphosphorylation and the Inability to Bind FBXO3. IScience *23*, 101491.

Wheway, G., Schmidts, M., Mans, D.A., Szymanska, K., Nguyen, T.-M.T., Racher, H., Phelps, I.G., Toedt, G., Kennedy, J., Wunderlich, K.A., et al. (2015a). An siRNA-based functional genomics screen for the identification of regulators of ciliogenesis and ciliopathy genes. Nat. Cell Biol. *17*, 1074–1087.

Wheway, G., Schmidts, M., Mans, D.A., Szymanska, K., Nguyen, T.-M.T., Racher, H., Phelps, I.G., Toedt, G., Kennedy, J., Wunderlich, K.A., et al. (2015b). An siRNA-based functional genomics screen for the identification of regulators of ciliogenesis and ciliopathy genes. Nat. Cell Biol. *17*, 1074–1087.

K Yusa, R Rad, J Takeda, A Bradley (2009) Generation of transgene-free induced pluripotent mouse stem cells by the piggyBac transposon. *Nat Methods* **6**, 363–369.

Zhang, S., Cooper Knock, J., Wemer, A., Shi, M. et al. (2022) Genome-wide identification of the genetic basis of amyotrophic lateral sclerosis. Neuron 110, 992–1008.

Declarations

Acknowledgements. We would like to acknowledge T. Yamomoto for the Multiplex CRISPR/Cas9 Assembly System Kit and S Park for the pDisplay plasmid obtained from Addgene. We would like to thank Allan Bradley for the plasmid and Shankar Srinivas for the pCagTag plasmid. The following antibodies were obtained from the Developmental Studies Hybridoma Bank, created by the NICHD of the

NIH and maintained at The University of Iowa, Department of Biology, Iowa City, IA 52242: 2H3 developed by Jessell, T.M. & Dodd, J. (HHMI/Columbia University), 40.2D6 developed by Jessell, T.M. & Brenner-Morton, S. (HHMI/Columbia University) and Rat401 (Nestin) developed by Hockfield, S. (Yale University School of Medicine). The research funded by a project grant from the Motor Neurone Disease Association (Project Grant 866-791) to VS.

Author contributions. The project was conceived by VS. VS and RF designed the experiments and RF performed the experiments. RF and VS analysed the data and wrote the manuscript.

Competing interests. The authors have no competing interests.

Materials & Correspondence. All correspondence and requests for Materials should be addressed to Dr Vasanta Subramanian (bssvss@bath.ac..uk)

Tables

Table 1: List of ES lines both wild type ad mutant ES cell lines used in the experiments

Identifier	Genotype	Clone IDs
CFAP410$^{WT/WT}$	Unmodified original ES cell line	R1 mESC
CFAP410$^{WT/HA}$	Heterozygous HA tag Knockin subclone of R1 (second allele remains WT)	I15
CFAP410$^{HA/HA}$	Homozygous HA tag Knockin subclone of R1	G24 & H13
CFAP410$^{WT/V20M-HA}$	Heterozygous V20M-HA tag, Subclone of I15 (second allele remains WT)	C13 & E09
CFAP410$^{V20M-HA/V20M-HA}$	Homozygous HA tag Subclone of H13	C15 & F02
CFAP410$^{WT/R73P-HA}$	Heterozygous R73P-HA tag, Subclone of I15 (second allele remains WT)	B24 & M04
CFAP410 $^{R73P-HA/ R73P-HA}$	Homozygous R73P-HA tag Subclone of H13	D14 & J13

Figures

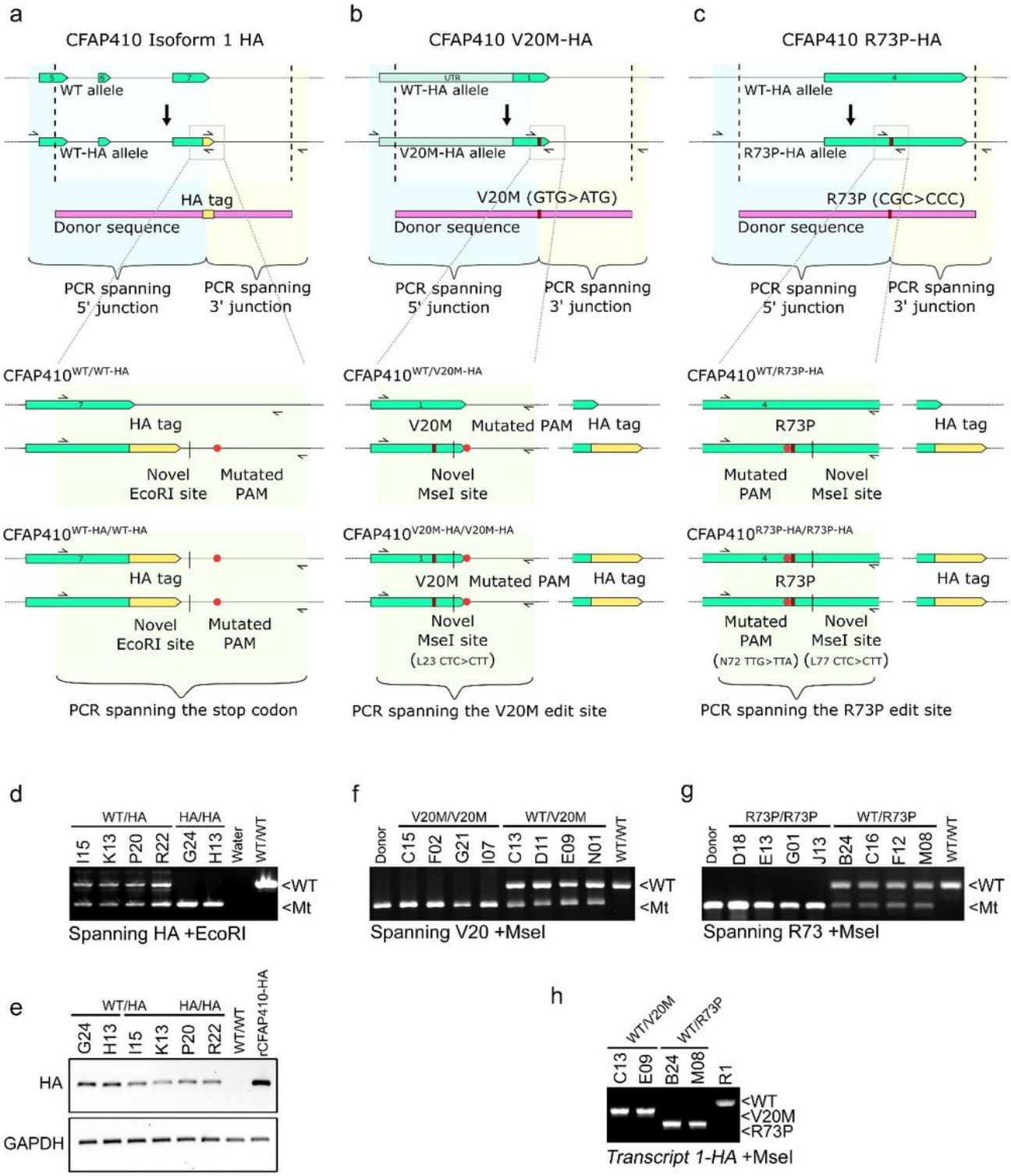

Figure 1

Sequential CRISPR/Cas9 gene editing the *CFAP410* locus to introduce an HA tag and point mutations

Nickase Cas9 and paired guide sgRNAs targeting the stop codon of *CFAP410* isoform 1 were used to mediate the introduction of a HA tag prior to the stop codon from a donor plasmid (a). The donor plasmid also carried a novel EcoRI site and mutated the PAM site for the 3' guide. A V20M or R73P point mutation (b & c) was then edited into clones characterised as either hetero (I15) or homozygously (H13) carrying the HA tagged allele. The donor plasmids carrying the V20M or R73P mutations also introduced synonymous base changes to leucine codons to create an MseI site, and mutated either the 3' (V20M) or 5' (R73P) PAM.

HA tag zygosity was determined by PCR across the locus followed by EcoRI digest (d). Western blot to show *CFAP410*-HA expression immunoblotted using anti-HA antibody (e). GAPDH as loading control and transgenic R1 overexpressing HA tagged human *CFAP410* used as a positive control (R1 hC21HA). V20M and R73P zygosity was determined by PCR across the locus followed by MseI digest (f & g). Donor plasmid and R1 ESC parent DNA was used as mutant (Mt) and wildtype (WT) controls. To determine whether heterozygous mutations were present in the HA tagged allele, RT-PCR was performed on HA-primed cDNA followed by MseI digest (h). Successful digestion indicated the point mutations were present on HA tagged allele.

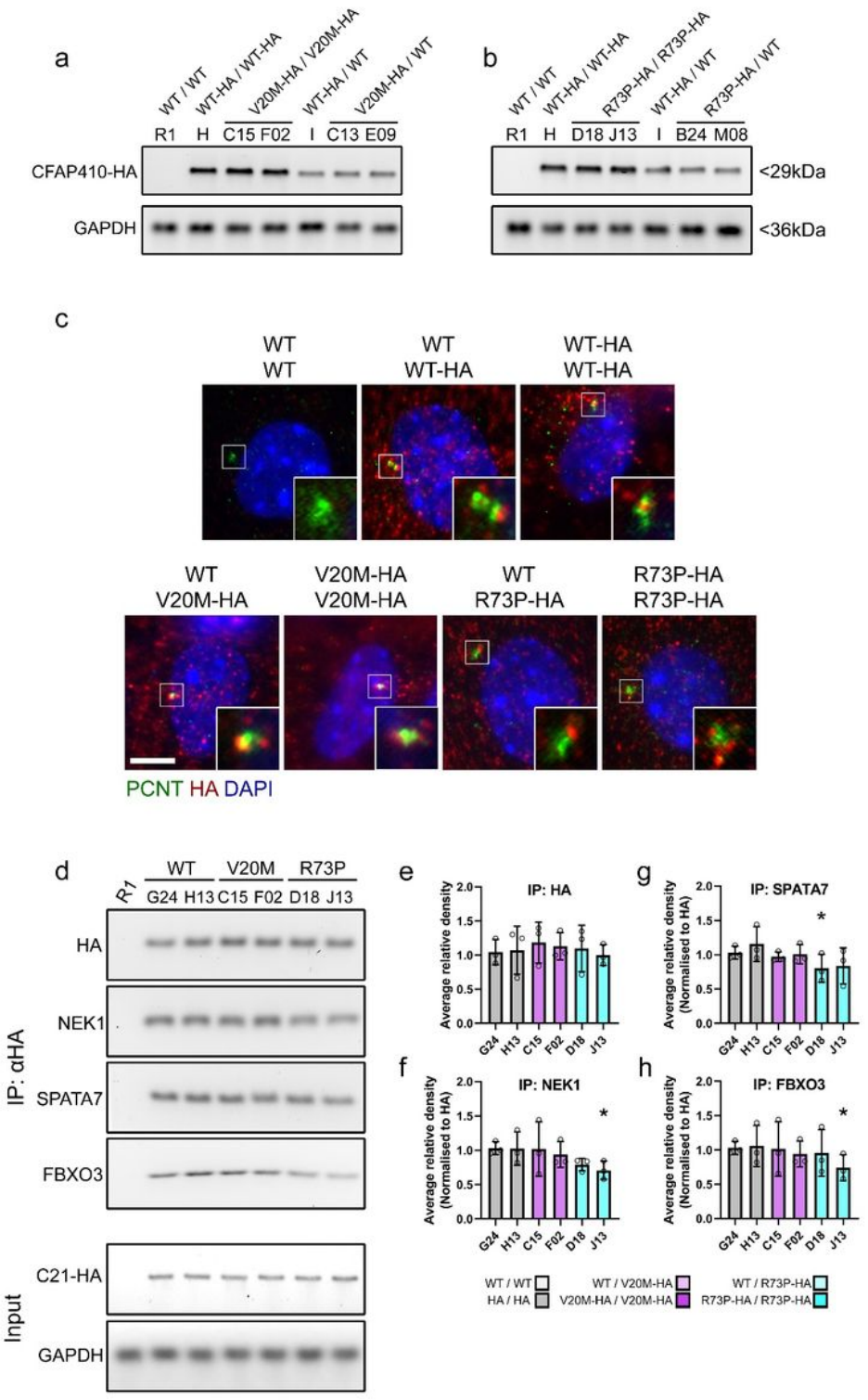

Figure 2

Expression of HA tagged *CFAP410* variants

Western blot of two representative clones from each genotype immunoblotted using anti-HA antibody (a). GAPDH as loading control. Immunostaining for PCNT and HA in representative clones counterstained with DAPI (b). Inset shows close crop of centrioles basal body. Scale bar 5μm.

(d) Co-immunoprecipitation using antibody against the HA tag and immunoblotting for NEK1, SPATA7 and FBXO3. Performed on neuronal culture lysates of R1 (*CFAP410*$^{WT/WT}$), G24 & H13 (*CFAP410*$^{WT\text{-}HA/WT\text{-}HA}$), C15 & F02 (*CFAP410*$^{V20M\text{-}HA/V20M\text{-}HA}$), D18 & J13 (*CFAP410*$^{R73P\text{-}HA/R73P\text{-}HA}$). Quantification of immunoprecipitated HA tagged *CFAP410* (e) and co-immunoprecipitated NEK1 (f), SPATA7 (g) and FBXO3 (h) from three replicate western blots (Means ±SEM). NEK1, SPATA7 and FBXO3 normalised to HA. * P<0.05.

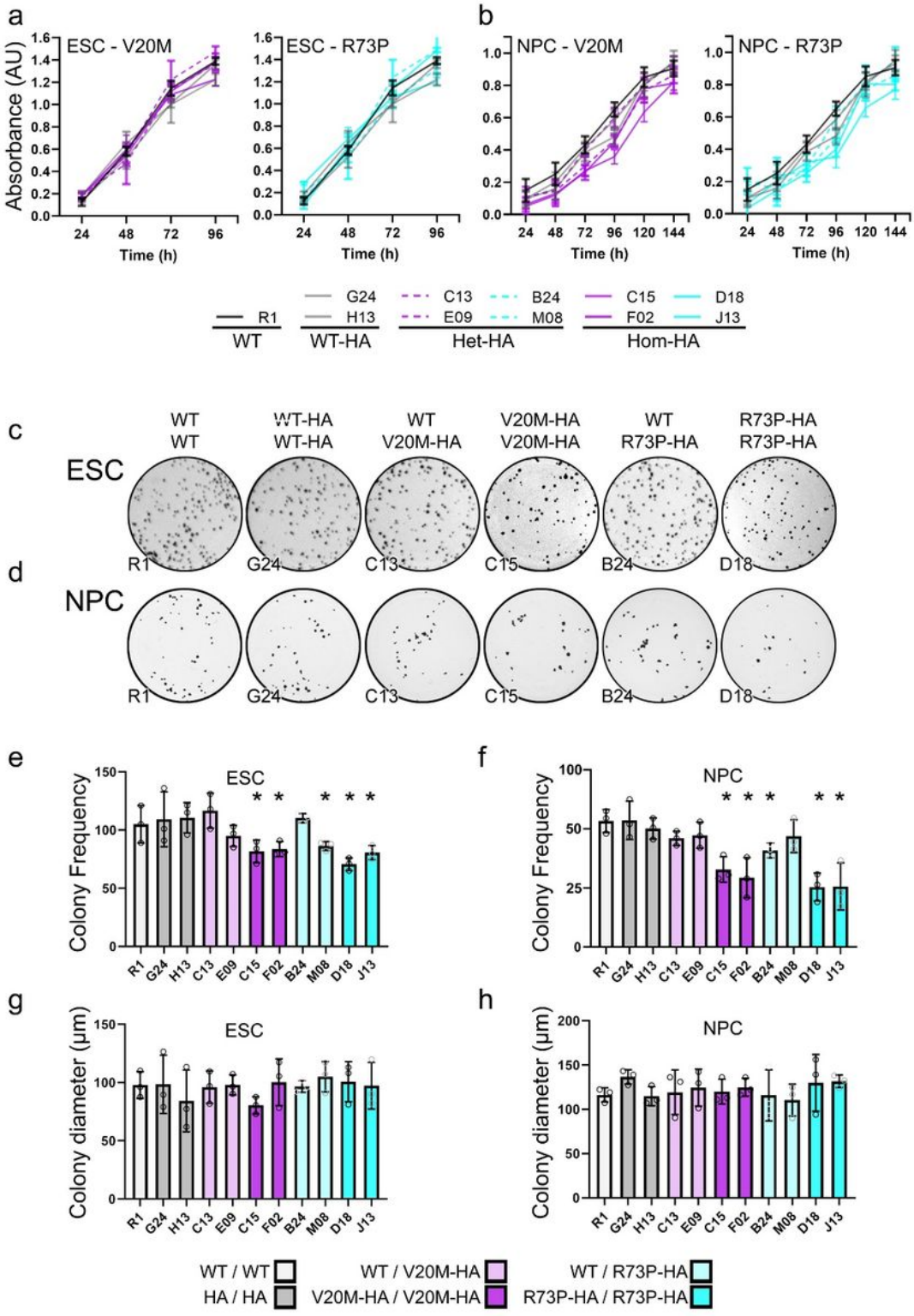

Figure 3

CFAP410 variants do not affect proliferation and growth of ESC or NPC but do affect survival

Proliferation was assayed over the indicated time courses with 24h intervals. Two clones of each ESCs (a) or NPCs (b) genotype were assayed alongside R1. Three experimental replicates performed with triplicate assay wells in each. Data presented as mean absorbance ±SEM.

Colony formation assays were performed also in triplicate with three replicates each of ESCs (c) and NPCs (d) of each genotype alongside R1 and stained with crystal violet. ESC and NPC colony frequency (e & f) was determined from each experiment and presented as mean frequency ±SEM. * $P<0.05$. ESC and NPC colony diameter (g & h) was determined from each experiment and presented as mean frequency ±SEM.

Key to genotypes: WT, *CFAP410*$^{WT/WT}$ (R1); WT-HA, *CFAP410*$^{WT\text{-}HA/WT\text{-}HA}$ (G24 & H13); Het-HA, *CFAP410*$^{WT/V20M\text{-}HA}$ (C13 & E09) and *CFAP410*$^{WT/R73P\text{-}HA}$ (B24 & M08); Hom-HA, *CFAP410*$^{V20M\text{-}HA/V20M\text{-}HA}$ (C15 & F02) and *CFAP410*$^{R73P\text{-}HA/R73P\text{-}HA}$ (D18 & J13).

a

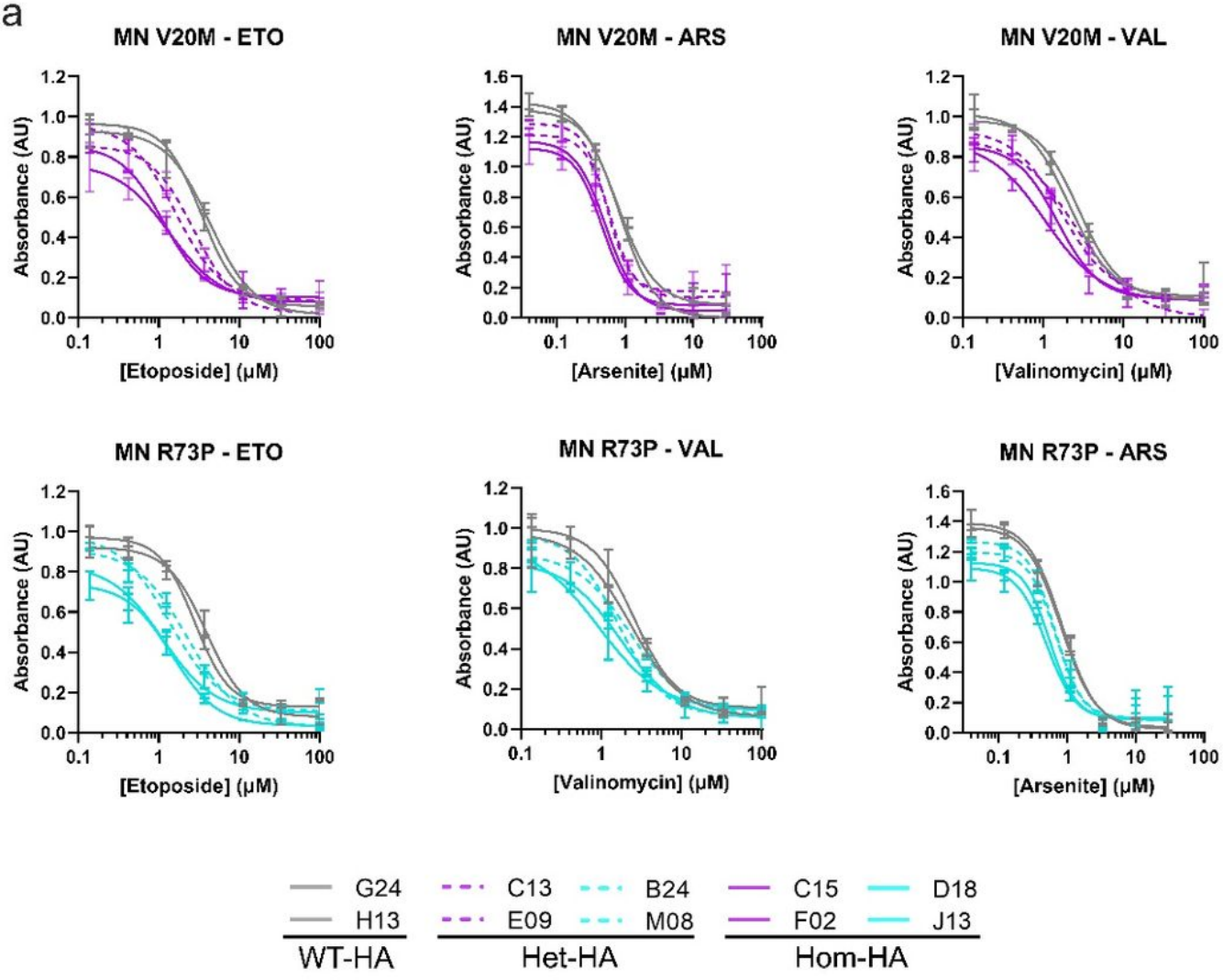

b

Genotype:		HA/HA		+/V20M-HA		V20M-HA/V20M-HA		+/R73P-HA		R73P-HA/R73P-HA	
Clone:		G24	H13	C13	E09	C15	F02	B24	M08	D18	J13
[EC50] µM:											
ESC	ETO	8.67	11.25	4.37	6.63	3.27	3.36	4.62	5.81	3.37	2.53
	VAL	7.79	6.20	4.85	6.87	2.85	3.97	4.75	4.53	2.95	3.71
	ARS	2.51	2.47	1.83	1.84	1.50	1.38	1.66	1.80	1.52	1.41
NPCs	ETO	8.75	11.81	4.76	6.91	4.09	2.62	4.36	7.17	3.66	3.21
	VAL	7.53	5.47	4.40	4.14	2.84	5.00	4.34	6.39	1.91	5.07
	ARS	2.66	2.92	2.07	1.81	1.54	1.56	1.86	2.02	1.45	1.35
Neurons	ETO	3.41	4.30	1.62	2.69	1.13	1.36	1.37	2.29	1.11	1.46
	VAL	2.77	2.11	1.70	2.57	1.06	1.52	1.65	2.35	0.94	1.77
	ARS	0.77	0.84	0.54	0.61	0.52	0.47	0.66	0.69	0.56	0.50

Figure 4

CFAP410 variants increase vulnerability to stress in differentiated neuronal cultures

(A) Kill curves of etoposide, valinomycin or sodium arsenite treated motor-neuron directed differentiation of *CFAP410* variants ESCs . Viability determined after 24h. Three experimental replicates performed with triplicate assay wells in each. Data presented as mean absorbance ±SEM. All X axes in log scale.

Concentrations of Drugs: Etoposide & Valinomycin 100.00, 33.33, 11.11, 3.70, 1.23, 0.41, 0.14 & 0.00µM, Sodium arsenite 30.00, 10.00, 3.33, 1.11, 0.37, 0.12, 0.04, 0.00µM.

Key to genotypes: WT, *CFAP410*$^{WT/WT}$ (R1); WT-HA, *CFAP410*$^{WT\text{-}HA/WT\text{-}HA}$ (G24 & H13); Het-HA, *CFAP410*$^{WT/V20M\text{-}HA}$ (C13 & E09) and *CFAP410*$^{WT/R73P\text{-}HA}$ (B24 & M08); Hom-HA, *CFAP410*$^{V20M\text{-}HA/V20M\text{-}HA}$ (C15 & F02) and *CFAP410*$^{R73P\text{-}HA/R73P\text{-}HA}$ (D18 & J13).

(B) summary table of EC50 concentrations for neurons, ESCs and NPCs determined from a 4-parameter nonlinear dose–response fitted curve. Full response curves for ESC and NPCs can be found in supplementary figure S6.

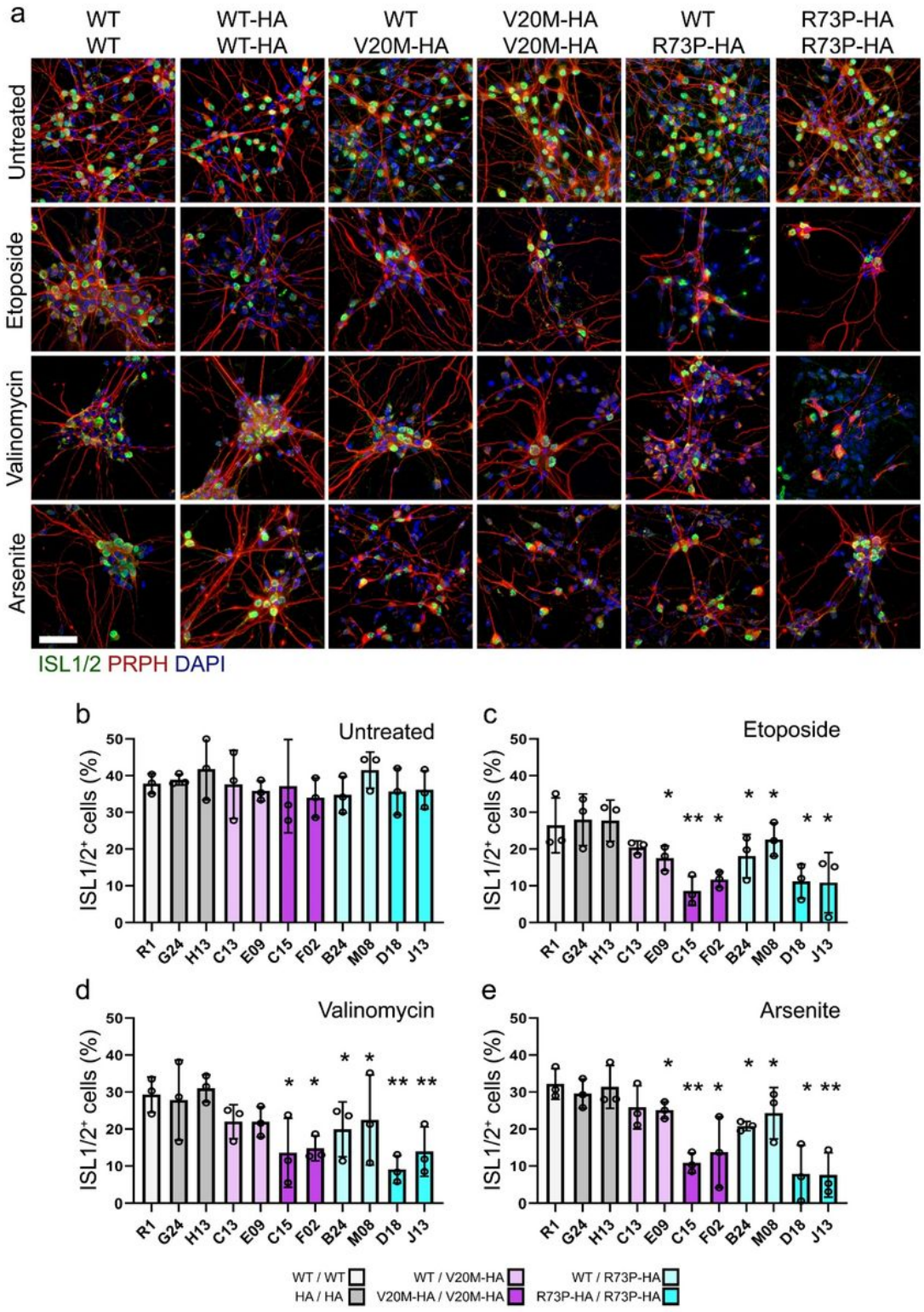

Figure 5

CFAP410 variant motor neurons are more vulnerable to genotoxic stress

(A) Immunostaining for the motor neuron markers islet1/2 and peripherin (ISL1/2, PRPH) in neuronal cultures differentiated from *CFAP410* variant ESC clones and treated with etoposide, valinomycin or

sodium arsenite for 24h. Representative images from a single clone of each genotype shown. Scale bar 50μm.

Average median Islet positive nuclei frequency was quantified from four random fields each from three experiments (Bar ±SEM, data points represent experimental medians) (B) without treatment, or in response to (C) etoposide, (D) valinomycin or (E) sodium arsenite. * P<0.05, ** P<0.005.

Key to genotypes: WT/WT, *CFAP410*$^{WT/WT}$ (R1); HA/HA, *CFAP410*$^{WT\text{-}HA/WT\text{-}HA}$ (G24 & H13); WT/V20M-HA, *CFAP410*$^{WT/V20M\text{-}HA}$ (C13 & E09); WT/R73P-HA, *CFAP410*$^{WT/R73P\text{-}HA}$ (B24 & M08); V20M-HA/V20M-HA, *CFAP410*$^{V20M\text{-}HA/V20M\text{-}HA}$ (C15 & F02); R73P-HA/R73P-HA, *CFAP410*$^{R73P\text{-}HA/R73P\text{-}HA}$ (D18 & J13).

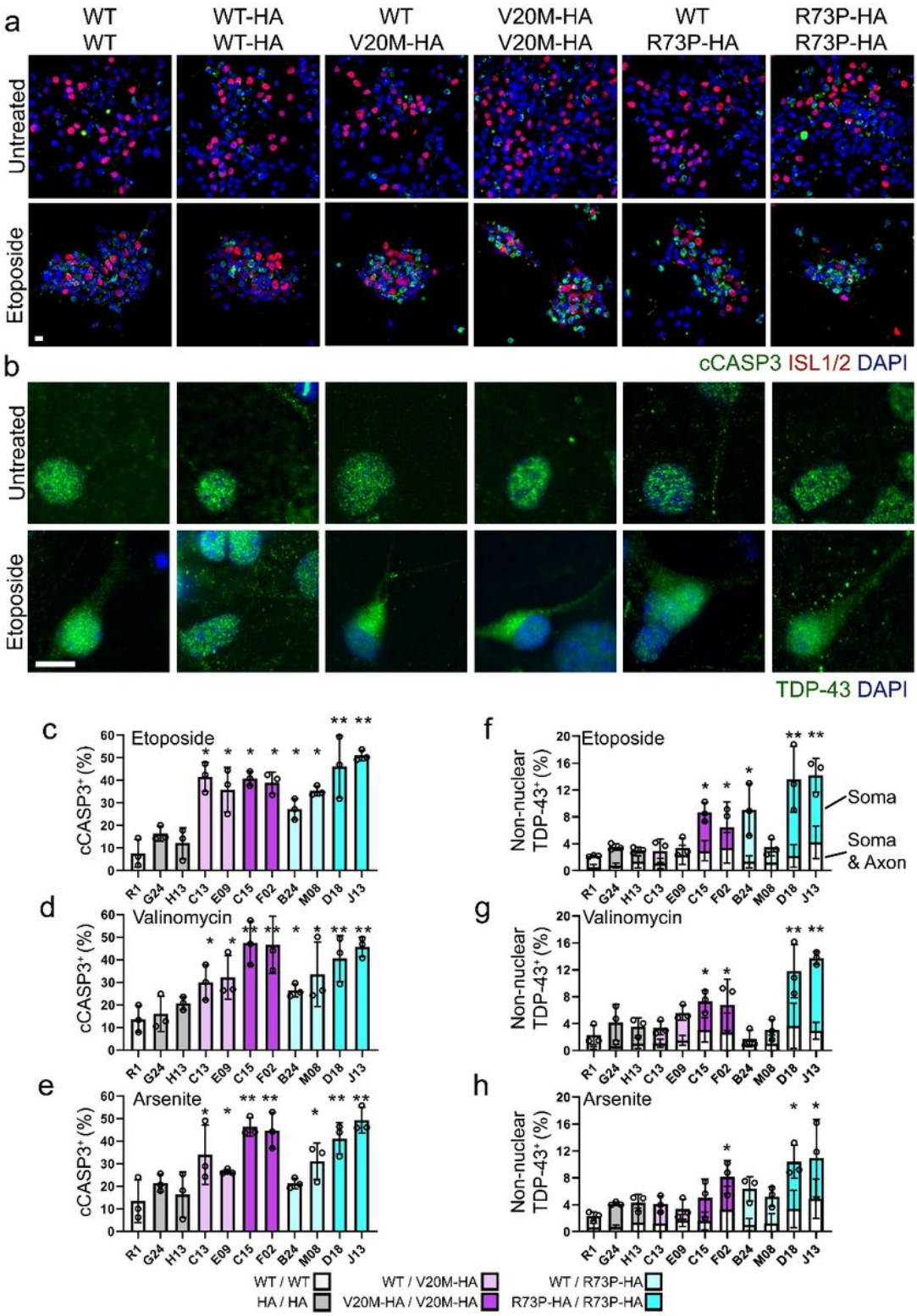

Figure 6

Increased apoptosis and TDP-43 redistribution in *CFAP410* variant neurons.

Immunostaining for (A) cleaved caspase 3 (cCASP2) and ISL1/2, or (B) TDP-43 in neurons differentiated from *CFAP410* variant ESCs and treated with etoposide for 24h. Representative images from a single clone of each genotype shown. Scale bar 10μm.

Average median cleaved caspase 3 positive nuclei frequency was quantified from four random fields each from three experiments (Bar ±SEM, data points represent experimental medians) in response to (C) etoposide, (D) valinomycin or (E) sodium arsenite. * P<0.05, ** P<0.005.

Cells with TDP-43 staining in the soma, or in the primary axon were quantified from four random fields each from three experiments (Bar ±SEM, data points represent experimental medians) in response to (F) etoposide, (G) valinomycin or (H) sodium arsenite . * P<0.05, ** P<0.005.

Immunostaining after treatment with valinomycin or sodium arsenite and quantification in untreated cells can be found in Figure S7.

Key to genotypes: WT/WT, *CFAP410*$^{WT/WT}$ (R1); HA/HA, *CFAP410*$^{WT\text{-}HA/WT\text{-}HA}$ (G24 & H13); WT/V20M-HA, *CFAP410*$^{WT/V20M\text{-}HA}$ (C13 & E09); WT/R73P-HA, *CFAP410*$^{WT/R73P\text{-}HA}$ (B24 & M08); V20M-HA/V20M-HA, *CFAP410*$^{V20M\text{-}HA/V20M\text{-}HA}$ (C15 & F02); R73P-HA/R73P-HA, *CFAP410*$^{R73P\text{-}HA/R73P\text{-}HA}$ (D18 & J13).

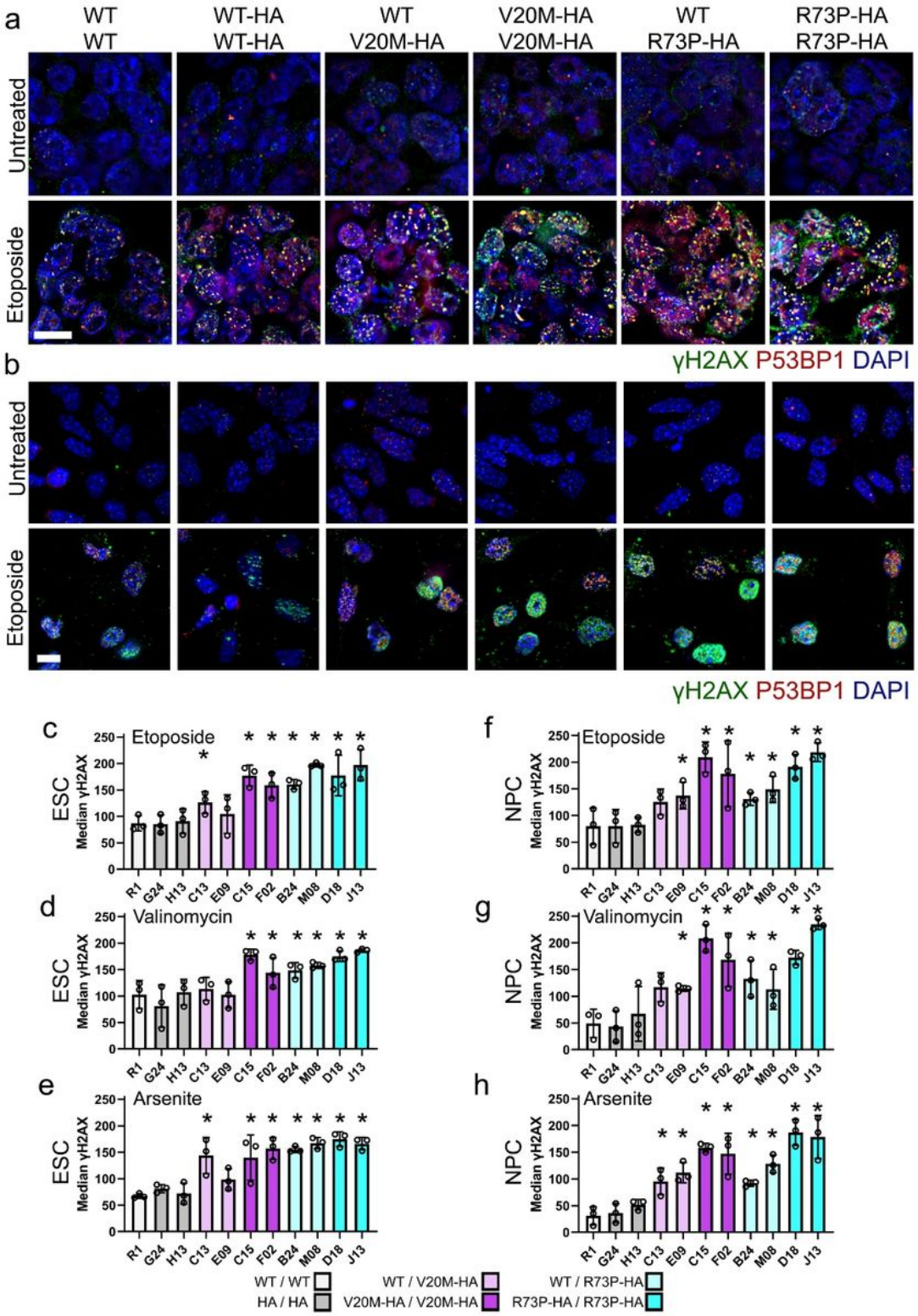

Figure 7

ESC and NPC lines carrying *CFAP410* variants show increased DNA damage response.

Immunostaining for γH2AX and P53BP1 in *CFAP410* variant ESCs (A) and NPCs (B) treated with etoposide for 24h. Representative images from a single clone of each genotype shown. Scale bar 10μm.

Average median nuclear γH2AX intensity in ESCs was quantified from four random fields each from three experiments (Bar ±SEM, data points represent experimental medians) in response to (C) etoposide, (D) valinomycin or (E) sodium arsenite. Average median nuclear γH2AX intensity in NPCs was quantified from four random fields each from three experiments (Bar ±SEM, data points represent experimental medians) in response to (F) etoposide ,(G) valinomycin or (H) sodium arsenite. * P<0.05.

Immunostaining after treatment with valinomycin or sodium arsenite and quantification of γH2AX in untreated cells can be found in **Figure S6**.

Key to genotypes: WT/WT, *CFAP410*$^{WT/WT}$ (R1); HA/HA, *CFAP410*$^{WT\text{-}HA/WT\text{-}HA}$ (G24 & H13); WT/V20M-HA, *CFAP410*$^{WT/V20M\text{-}HA}$ (C13 & E09); WT/R73P-HA, *CFAP410*$^{WT/R73P\text{-}HA}$ (B24 & M08); V20M-HA/V20M-HA, *CFAP410*$^{V20M\text{-}HA/V20M\text{-}HA}$ (C15 & F02); R73P-HA/R73P-HA, *CFAP410*$^{R73P\text{-}HA/R73P\text{-}HA}$ (D18 & J13).

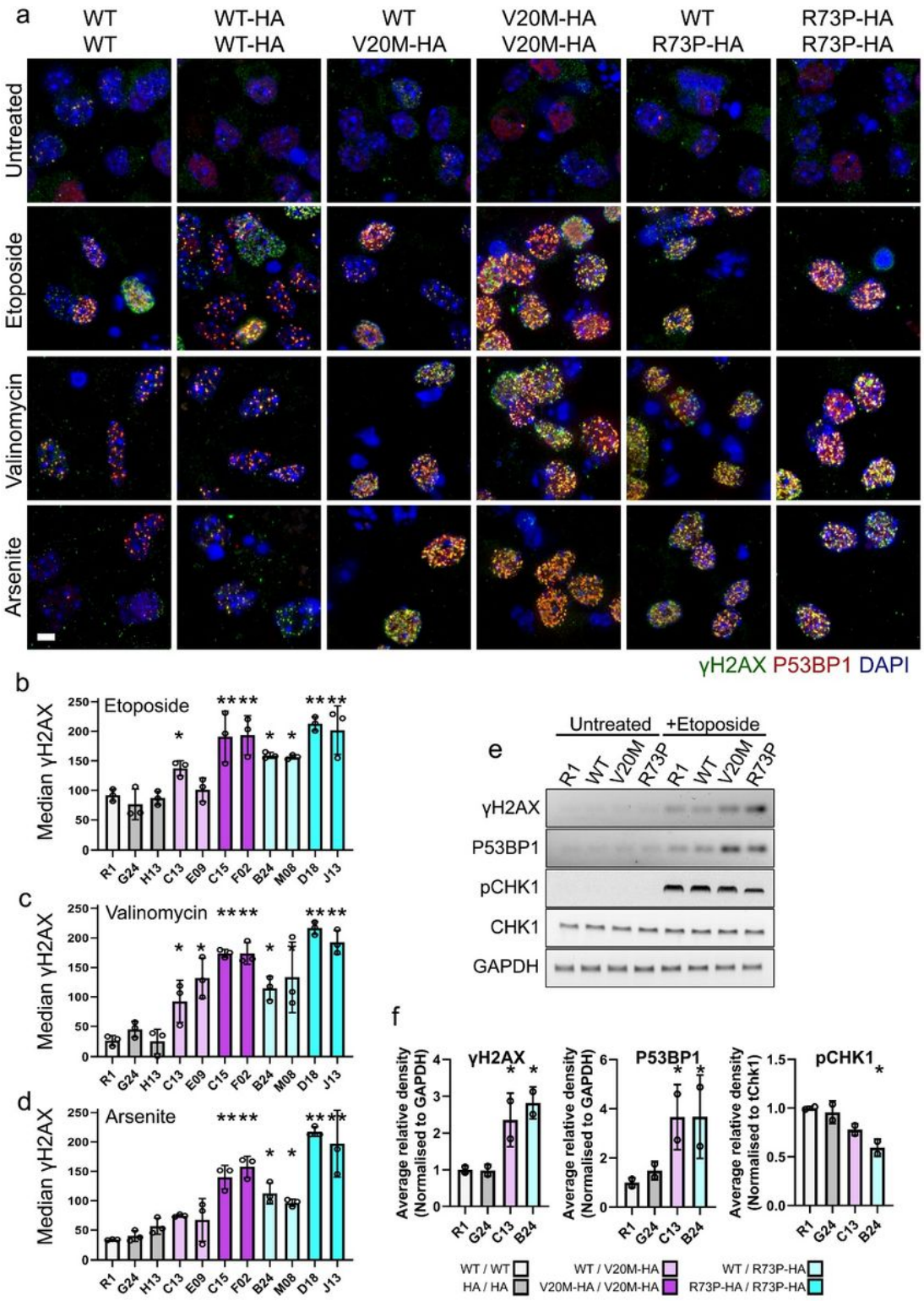

Figure 8

Neurons carrying *CFAP410* variants show increased DNA damage response.

(A) Immunostaining for γH2AX and P53BP1 in neurons differentiated from *CFAP410* variant ESCs and treated with etoposide, valinomycin or sodium arsenite for 24h. Representative images from a single clone of each genotype shown. Scale bar 10μm.

Average median nuclear γH2AX intensity in neurons was quantified from four random fields each from three experiments (Bar ±SEM, data points represent experimental medians) in response to (B) etoposide, (C) valinomycin or (D) sodium arsenite (d). * P<0.05, ** P<0.005. Quantification of γH2AX in untreated cells is shown in **in Figure S6**.

(E) Representative Western blot of untreated and etoposide treated cells for γH2AX, P53BP1, phospho & total CHK1. GAPDH loading control. (F) quantification of two replicate western blots for γH2AX, P53BP1 (normalised to GAPDH), and pCHK1 (normalised to total CHK1).

Key to genotypes: WT/WT, *CFAP410*$^{WT/WT}$ (R1); HA/HA, *CFAP410*$^{WT\text{-}HA/WT\text{-}HA}$ (G24 & H13); WT/V20M-HA, *CFAP410*$^{WT/V20M\text{-}HA}$ (C13 & E09); WT/R73P-HA, *CFAP410*$^{WT/R73P\text{-}HA}$ (B24 & M08); V20M-HA/V20M-HA, *CFAP410*$^{V20M\text{-}HA/V20M\text{-}HA}$ (C15 & F02); R73P-HA/R73P-HA, *CFAP410*$^{R73P\text{-}HA/R73P\text{-}HA}$ (D18 & J13).

Supplementary Files

This is a list of supplementary files associated with this preprint. Click to download.

- Supplementaltablesgelsandblotimages060522.docx